

Article

The Impact of Asymmetric Contact Resistance on the Operating Parameters of Thermoelectric Systems

Ryszard Buchalik ¹, Grzegorz Nowak ^{1,*} and Iwona Nowak ²

¹ Department of Power Engineering and Turbomachinery, Silesian University of Technology, Konarskiego 18, 44-100 Gliwice, Poland; ryszard.buchalik@polsl.pl

² Department of Applications of Mathematical and Artificial Intelligence Methods, Silesian University of Technology, Kaszubska 23, 44-100 Gliwice, Poland; iwona.nowak@polsl.pl

* Correspondence: grzegorz.nowak@polsl.pl

Abstract: This paper presents a simulation model for a system equipped with thermoelectric elements, considering the impact of independent thermal contact resistances on each side of the module. An analytical model was constructed, taking into account the asymmetry of thermal resistances between the generator/cooler and the respective heat source/heat sink. A comparative analysis of thermoelectric device operating indicators such as conducted heat, efficiency, and the electricity/cooling power produced was performed. The selection of electrical current in the circuit was analysed based on the maximization of power or efficiency. This paper discusses deviations from ideal conditions, specifically the absence of thermal resistance between the heat source/sink and the thermoelectric junction. The model accurately simulates the operating conditions of the thermoelectric system with a low computational cost. The results indicate that the total thermal resistance, rather than its location, predominantly affects the operation of the thermoelectric generator. However, in cooling operations, the influence of thermal resistance significantly depends on the cooling power demand and temperature.

Keywords: TEG; TEC; heat resistance; thermoelectric module; heat transfer



Citation: Buchalik, R.; Nowak, G.; Nowak, I. The Impact of Asymmetric Contact Resistance on the Operating Parameters of Thermoelectric Systems. *Energies* **2024**, *17*, 599. <https://doi.org/10.3390/en17030599>

Academic Editor: Mahmoud Bourouis

Received: 31 December 2023

Revised: 14 January 2024

Accepted: 24 January 2024

Published: 26 January 2024



Copyright: © 2024 by the authors. Licensee MDPI, Basel, Switzerland. This article is an open access article distributed under the terms and conditions of the Creative Commons Attribution (CC BY) license (<https://creativecommons.org/licenses/by/4.0/>).

1. Introduction

The rationalization of energy consumption and the utilization of waste energy released in various thermal processes have become essential over the past few years. One of the methods to recover waste energy is the use of thermoelectric generators (TEGs), which convert heat flow directly into electricity [1]. The efficiency of such an energy conversion is relatively small and is significantly dependent on the effective temperature difference at the thermoelectric junctions. The temperature difference is highly influenced by the heat transfer intensity at both sides of the TEG, which means the thermal resistance between the heat source/sink and the junctions. Many analyses of the thermal state of TEGs neglect heat resistance or assume that it is equal on both sides of the thermoelectric module (TEM). While the first assumption may lead to a significant discrepancy with the actual situation, the second should be justified.

One of the mentioned approaches is to consider only the TEG with specific temperatures of the hot and cold junction [2]. This is tantamount to idealizing the boundary conditions on the TEG surface, implying perfect contact (no thermal resistance) between the thermoelectric module casing and the heat source/sink. Thus, the temperature of the thermoelectric junction is the same as the temperature of the respective heat reservoir. In this case, Marchenko conducted an in-depth theoretical study of the heat transfer problem using thermoelectric legs [3]. He compared several methods for the heat conduction solution within the legs and concluded that the error in the approximated solutions increases with increasing Joule and Thomson effects. An extension of this approach is to consider the

thermal conductivity of the module housing with the specified heat source/sink temperature and the contact resistance between the heat exchangers and the TEG. The resistance distribution is primarily symmetrical, that is, identical on both sides of the thermoelectric generator.

Kim [4] considered the thermal resistance of contact layers and derived the actual temperature difference at the thermoelectric junctions with known symmetrical thermal resistances on both sides of the TEG. Lv et al. [5] analysed all heat transfer paths between sources, with a focus on minimizing the heat losses resulting from convection and radiation. The authors indicated that limiting internal heat loss may improve the TEG efficiency by no more than about 9%. Youn et al. [6] considered the problem of thermal resistance in simple electronic applications. They addressed the maximum power shift from the typical impedance-matching condition (equal load and internal electrical resistances) caused by thermal resistance at the contact surfaces. The influence of parameters that determine the heat resistance in the thermal interface material is presented in [7]. The authors analysed the surface finish and clamping force and showed to what extent they affect the TEG performance. In addition, in some works, a combination of different materials within one leg is discussed [8], also in combination with a variable cross-section of the legs [9].

The heat utilized for TEG operation originates from various sources. In their study [10], the authors focused on a system where the heat source for the TEG is a hot gas flow, and the performance of the system is influenced by the flow parameters. Numerous recent papers delve into issues related to TEG application in the automotive industry, with exhaust gases used as a heat source before releasing them into the environment [11] or heat harvested from the cooling system [12]. Further efforts to enhance heat exchange by modifying the heat exchanger's geometry are discussed in [13,14]. Zaher et al. [15] developed a TEG-integrated numerical model of a heat exchanger designed to capture waste heat from gas-fired devices in the food industry. They assessed the impact of axial heat conduction in a multi-row heat exchanger. Paper [16] presents an analysis of the use of thermal radiation focused on lenses in a heating furnace. The growing use of photovoltaic panels has spurred researchers' interest in hybrid PV-TEG systems. The PV module in such a system serves as the upper heat source for the TEG. Paper [17] presents an assembly of a concentrated photovoltaic (CPV) cell and a TEG. Some authors attempt to use advanced algorithms to find the optimal solution to the geometry and operating point of a thermoelectric cell [18]. The authors of [19] suggest the use of phase change materials on the cold side of the thermoelectric module to improve energy conversion efficiency. This resulted in a several-percent increase in the PV-TEG system power. The issue was further explored in [20]. Bjørk and Nielsen [21] explore a tandem PV-TEG system, directing short-wave radiation onto the PV cell and long-wave radiation onto the TEG module. The authors emphasize that the influence of this configuration on the overall system efficiency is relatively negligible. Using a slightly different approach, [22] investigates hybrid PV-TEG systems, with a specific focus on evaluating how module geometry affects efficiency. In addition to converting waste heat into electricity, thermoelectric modules can also be easily used as a heating or cooling element [23] supplied with electricity.

Heat recovery is no longer the domain of large industrial systems alone—it is also commonly used in microscale processes [24]. Today, we are surrounded by devices that require very little energy (e.g., wearable) and can be powered by a small electric generator, and one way of using small sources of heat, which is frequently waste heat, is to utilize TEGs. The development of the smart things industry also leads to the search for different forms of powering devices with low energy demand [25]. It also requires research on the power sources' durability, including thermoelectric generators [26]. Moreover, in “zero energy” buildings, thermoelectric modules can be widely used, both as generators and/or heat pumps [27]. Thermoelectric systems can also be used in electronics cooling [28] to control operating conditions.

Thermoelectric modules find another application in their cooling mode (thermoelectric cooler—TEC). The use of such devices is becoming increasingly common across various

technological fields. A common application involves incorporating thermoelectric cells in consumer refrigerators [29], where they help maintain a consistent temperature for electronic components [30] or in systems designed to prevent the development of thermal stresses [31]. One notable advantage of thermoelectric cells is their versatility. In addition to operating in heat pump mode, they can also function as electricity generators by harnessing a temperature gradient, converting a portion of the heat flux into electrical energy [32]. However, the broader adoption of thermoelectric modules is hindered by their relatively low energy conversion efficiency when operating as generators and a low coefficient of performance (COP) in the heat pump mode. The imperative to enhance efficiency is evident in vigorous development efforts, encompassing the exploration of new thermoelectric materials and the refinement of thermoelectric cell properties [33,34], as well as decreasing the existing constraints (i.e., in heat transfer).

TECs can also be used to induce the phenomenon known as supercooling [35], where a momentary reduction in the temperature of the cooled space occurs below the minimum value attainable in a steady state. The degree of supercooling and the cooling power at hand are contingent on the contact heat resistance between the thermoelectric junction and the surroundings. It is essential to explore the extent to which the operation of a TEC is affected by thermal resistance.

The contribution of this paper, compared with the works published so far by other authors, is the attempt to analyse TEG and TEC operation taking account of the contact thermal resistance of the accompanying elements in the most extended form, i.e., with independent values of resistance on the TEG/TEC cold and hot sides. It is taken into account that thermal resistance can be created by elements of the TEG/TEC structure itself (e.g., the ceramic layer), the heat-conducting grease layer, the surface film conductance, etc. Moreover, the contact quality, and thus, the heat resistance, may change with time, and these changes may occur differently for low and high operating temperatures.

2. Theoretical Model

The Seebeck phenomenon is based on electromotive force generation, while the joints of two connected thermoelectric materials are kept at different temperatures. For a given thermoelectric module (material pair), its electromotive force is a function of the difference between the temperatures of the junctions ($EMF = \alpha(T_h - T_c)$). Therefore, it is important to know this quantity from the point of view of the achieved useful electrical parameters. The TEG electric circuit is electrically isolated from heating/cooling surfaces so that individual couples should not be short-circuited accidentally. Unfortunately, electrical insulation creates an additional thermal barrier between the heat source or heat sink and the TEG junctions. Generally, for most materials, the conduction of electricity is directly linked to the conduction of heat, so it is hard to find the desired materials, in this case—the electrical insulator and a good thermal conductor. Usually, there is also a need for thermal interface material between the thermoelectric module case and the heat source/sink. As a result, the operating temperatures of the thermoelectric junctions differ from the temperatures of the exchangers. These differences will increase with the weakening of the thermal contact between the TEG surfaces and the heat source/sink. The typical ceramic cover of the thermoelectric module is coated on the outside with a heat-conducting grease, the purpose of which is to reduce resistance between the heat exchanger and the ceramic housing. Contact resistance will therefore be a function of the parameters of the grease itself and also of the degree to which the grease fills the irregularities in the contacting surfaces, surface smoothness, and of the housing conductivity. Time changes in the physical properties of grease are also significant. They may have a substantial impact on the contact resistance between the heat exchanger and the module surface depending on the operating temperature, as well as the device in-service time and the grease structural changes related thereto. Because the surfaces of the thermoelectric modules usually have significantly different temperatures, the thermal resistance on the two sides can differ to a great extent and have a vital influence on the overall system characteristics. Since the aim of this research

is to show the influence of thermal resistance on the thermoelectric module performance in a comparative way, rather than determine their absolute parameters, the material properties are assumed to be temperature independent.

Figure 1 illustrates the basic idea of the model used. The thermoelectric module is placed between the heat sources/sinks with temperatures T_{ha} and T_{ca} , respectively. Due to the thermal resistance between the surfaces of the heat exchangers and the TEG junctions (r_{sh} and r_{sc}), the hot junction temperature is lower than the temperature of the exchanger ($T_h < T_{ha}$), whereas the cold junction temperature is higher ($T_c > T_{ca}$) in the case of generators and opposite ($T_h > T_{ha}$ and $T_c < T_{ca}$) in the case of cooler. In this way, depending on the resistance value, a part of the system exergy is lost.

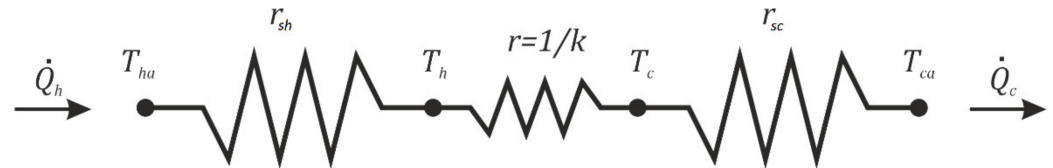


Figure 1. Thermal path of the TEG system.

The analysis starts from the principle of energy conservation for the TEM, according to which:

$$\dot{Q}_h = \dot{Q}_c + P_{TEG}, \quad (1)$$

where \dot{Q}_h and \dot{Q}_c denote supplied and released heat, respectively, and P_{TEG} is the electric power consumed in the external receiver (or supplied in the case of TEC (heat pump) operation). The power can be expressed as:

$$P_{TEG} = VI, \quad (2)$$

where V is the voltage on the external TEG wires and I is the circuit current.

By carrying out the energy balance for the upper and lower surfaces between the thermoelectric module and the heat source/sink, as well as the energy balance of the module itself, and considering the thermal resistance between thermoelectric junctions and heat exchangers, the following can be written:

$$k(T_h - T_c) + \alpha IT_h - \frac{I^2 R}{2} = \frac{(T_{ha} - T_h)}{r_{sh}} = \dot{Q}_h, \quad (3)$$

$$k(T_h - T_c) + \alpha IT_c + \frac{I^2 R}{2} = \frac{(T_c - T_{ca})}{r_{sc}} = \dot{Q}_c. \quad (4)$$

On the left side of the equations successively appear heat conducted by thermoelectric legs of thermal conductivity k , Peltier heat, and Joule heat [36]. The heat conducted between the junction and the corresponding exchanger (the right-hand side equality sign of above equations) is represented by the ratio of the temperature difference at the layer to the thermal resistance of the layer. The model assumes that on both sides of the module, there are independent values of thermal resistance (r_{sh} and r_{sc}). In other words, r_{sh} and r_{sc} are proportionality coefficients between heat transferred through the surface and the temperature difference. The Peltier coefficient is expressed as a product of the Seebeck coefficient and absolute temperature ($\pi = \alpha T_{h,c}$), and R stands for the internal electrical resistance of the thermoelectric module. Assuming that the material properties are temperature-independent, the Thomson effect will not occur.

Based on the relations presented above, it is possible to derive the relation describing the temperature gradient on the thermoelectric junction:

$$T_h - T_c = \frac{2\alpha I^3 R r_{sh} r_{sc} + 2\alpha I (r_{sc} T_{ha} + r_{sh} T_{ca}) + I^2 R (r_{sc} - r_{sh}) + 2(T_{ca} - T_{ha})}{2(\alpha^2 I^2 r_{sh} r_{sc} + \alpha I (r_{sc} - r_{sh}) - k(r_{sc} + r_{sh}) - 1)}. \quad (5)$$

The above formula can be combined with the relation describing Ohm's law and voltage resulting from the Seebeck coefficient:

$$V = \alpha(T_h - T_c) - RI. \quad (6)$$

This formula can be simplified for short-circuit conditions (taking $V=0$). This leads to the following quadratic equation for current:

$$\alpha I^2 R(r_{sc} - r_{sh}) - 2I(\alpha^2(r_{sc}T_{ha} + r_{sh}T_{ca}) + kR(r_{sh} + r_{sc}) + R) + 2\alpha(T_{ha} - T_{ca}) = 0, \quad (7)$$

whose discriminant totals:

$$\Delta = 4(\alpha^2(r_{sc}T_{ha} + r_{sh}T_{ca}) + kR(r_{sh} + r_{sc}) + R)^2 - 8\alpha^2 R(r_{sc} - r_{sh})(T_{ha} - T_{ca}), \quad (8)$$

and can be used to determine the TEG short-circuit current as one of Equation (7)'s roots (the other is non-physical):

$$I_{SC} = \frac{2(\alpha^2(r_{sc}T_{ha} + r_{sh}T_{ca}) + kR(r_{sh} + r_{sc}) + R) - \sqrt{\Delta}}{2\alpha R(r_{sc} - r_{sh})}. \quad (9)$$

The authors of [6] assumed that the term $\alpha I^2 R(r_{sc} - r_{sh})$ in (7) is sufficiently small to neglect it and consider this equation in a linear form. Here, we take into account the full form of (7) and observe the influence of asymmetric contact on the thermoelectric module performance.

Formulas describing the current magnitude corresponding to the maximum efficiency and maximum power can be delivered analytically; however, its form and complexity make it moderately useful. Assuming that the current corresponding to the maximum power is half of the short-circuit current, the equation describing the maximum useful power of the thermoelectric generator takes the following form:

$$P_{TEG}^{max} = \frac{I_{SC} [4I_{SC}(\alpha^2(r_{sc}T_{ha} + r_{sh}T_{ca}) + kR(r_{sc} + r_{sh}) + R) + \alpha I_{SC}^2 R(r_{sh} - r_{sc}) + 8\alpha(T_{ca} - T_{ha})]}{4(\alpha^2 I_{SC}^2 r_{sh} r_{sc} + 2\alpha I_{SC}(r_{sc} - r_{sh}) - 4k(r_{sh} + r_{sc}) - 4)} \quad (10)$$

The model is valid only for $r_{sh} \neq r_{sc}$ as there is a singularity in I_{SC} when $r_{sh} = r_{sc}$ (Equation (9)). This issue can be numerically addressed using slightly different values for thermal resistances, or one can opt for a much simpler model when $r_{sh} = r_{sc}$ [36]. However, this problem does not arise in the numerical solutions.

The thermoelectric generator efficiency is defined as the useful power-to-absorbed heat flow ratio, and in this case, it is expressed as:

$$\eta = \frac{P_{TEG}}{\dot{Q}_h}. \quad (11)$$

Putting aside a specific thermoelectric module, the impact of thermal resistance on the TEM two sides on the device performance can be formulated based on the material properties of the TEM junctions and the TEM geometry. The internal electrical resistance of a TEG can be defined based on specific resistance (ρ_m) and the leg's dimensions (assumed rectangular cuboid):

$$R = \frac{\rho_m n h}{A}, \quad (12)$$

where n is the number of thermoelectric legs and h and A are the height and the cross-sectional area of the leg, respectively. The TEM thermal conductivity can be written using the thermal conductivity of the thermoelectric material (λ_m):

$$k = \frac{\lambda_m n A}{h}. \quad (13)$$

The TEG Seebeck coefficient is described in the same manner, with α_m representing difference in Seebeck coefficients for a single thermoelectric couple:

$$\alpha = \frac{\alpha_m n}{2} . \quad (14)$$

A similar method can be applied to express the contact layer resistance, relating it to the unit of the surface area.

$$r_{sh, sc} = \frac{r_{h,c}}{nA f_A} , \quad (15)$$

where f_A is a factor that correlates the total leg area and the substrate area. This approach is useful for optimization where the TEG structure changes.

3. Numerical Models

Appropriate computational models were prepared to evaluate the effect of the magnitude of thermal resistance and its asymmetry on both sides of the thermoelectric generator. The first is a one-dimensional numerical model, which is based on the analytical formulation presented above. The second model was prepared based on the finite element method in a 3D configuration.

3.1. One-Dimensional Numerical Model

Using the presented analytical model, a computer program was developed to simulate the operation of the TEM system [37]. The algorithm input data, apart from the material parameters and geometrical features of the TEM, are the heat source/heat sink temperatures in the case of TEG and ambient temperatures and heat transfer factors in the case of TEC, the independent values of thermal resistance on the TEG hot and cold side and the current in the circuit. Based on this, the temperature difference on the thermoelectric junction, the voltage on the TEG terminals, the power output, and the power and voltage on internal resistance are calculated. In the next step, the TEG or TEC efficiency is calculated, and the efficiency is compared to the Carnot cycle for temperatures of the heat source and heat sink, heat on both sides of the TEG, and *EMF* for the open- (*oc*) and short-circuit (*sc*) states. By performing calculations for different currents flowing in the circuit between the *oc* and the *sc* state, the full operating characteristics of the thermoelectric generator can be determined. Moreover, by varying any input parameter, e.g., thermal resistance, it is possible to observe its impact on TEG performance.

3.2. FEM Model

The FEM model (Figure 2) of the thermoelectric module was prepared in Ansys 2023R2 for a real, commercially available TEG. It consists of 199 thermoelectric couples made of *n* and *p* semiconductors and connections between them. Actual geometry data, based on our own measurements, were used for all module elements. The module is encapsulated on both sides by a ceramic layer. A thin layer of a material with controlled thermal conductivity is modelled next to it to substitute for the contact thermal resistance between the heat exchangers and the thermoelectric module. The layer's thermal conductivity can be varied independently on either side of the module.

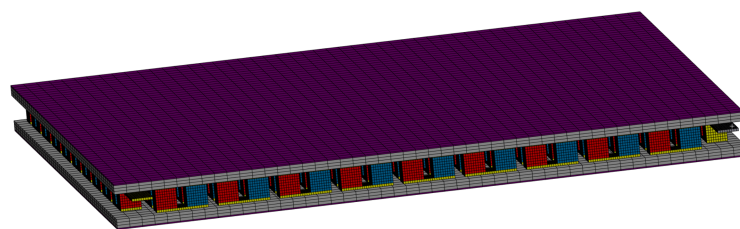


Figure 2. FEM model of the thermoelectric module.

The geometric model was discretized using over 360 thousand nonlinear finite elements, resulting in slightly over 1.86 million nodes in the numerical mesh.

A constant temperature condition was established on the upper and lower surfaces of the structure to simulate generator operation (TEG). Heat flow through the module is primarily attributed to conduction alone, and all surfaces not in contact with other elements (i.e., side walls of the thermoelectric legs) are treated as adiabatic. At one of the TEG terminals, zero voltage was set, while the assumed current value was specified to reflect various operating conditions of the TEG. Based on temperature difference and flowing current, results for the amount of heat exchanged, electrical power, and temperature field throughout the module are obtained.

4. Theoretical Model

The prepared numerical tools were used to simulate the TEM system under different operating conditions resulting from the different side placement of thermal resistance between the module and the heat exchangers. The thermal resistance of the contact layer used for the simulation results from a series of our own experimental tests carried out for commercially available TEGs. It represents the total thermal resistance between the thermoelectric junction and the respective heat reservoir. It was determined under a clamping force of 100 N for a 50×50 mm module. In the experiment, it was assumed that the resistance was uniform on both sides of the module. The corresponding value is then $220 \mu\text{K}\cdot\text{m}^2/\text{W}$. For the subsequent simulations, it was assumed that the resistance of each of the two layers could be set independently to a relatively high real value ($220 \mu\text{K}\cdot\text{m}^2/\text{W}$) or a hypothetical value of 0, indicating no thermal resistance at all.

The calculations were carried out for the MULTICOMP PRO MCTE1-19913L-S module, whose parameters were determined based on our own measurements. The first investigated situation concerns electricity generation using a heat source and a heat sink with different temperatures (120°C and 20°C). Based on the measurement technique presented in [36], the following values of the Seebeck coefficient for the thermoelectric leg, thermal conductivity, and specific electrical resistance were used for the calculations: $\alpha_m = \pm 0.22 \text{ mV/K}$, $\lambda_m = 2.74 \text{ W/(mK)}$, and $\rho_m = 6.60 \mu\Omega\text{m}$, respectively. The parameters are assumed to be temperature-independent. The module considered consists of $n = 398$ legs (199 thermoelectric couples) with a height of $h = 1.5 \text{ mm}$. The surface area of the module is $A_{\text{module}} = 25 \text{ cm}^2$ and the leg cross-section is a square with a 1.65 mm side length.

4.1. FEM Simulations

First, selected cases of module operation were simulated using the 3D FEM model. The purpose was to compare the 3D numerical model with a one-dimensional solution. The FEM calculations provide a complete picture of the thermal and electric fields for different operating conditions of the TEG module. Simulations were carried out for the TEM data mentioned above, and the results were compared to the 1D solution. Example results for the case where the contact resistance occurs only on the module hot side are shown in Figures 3–5 for the electric current value corresponding to the highest achievable electric output power. In the absence of contact resistance on the TEG cold side, the cold junction temperature is practically the same as the heat sink temperature. On the hot side, a significant decrease in the junction temperature is observed compared with the heat source temperature (chart in Figure 3).

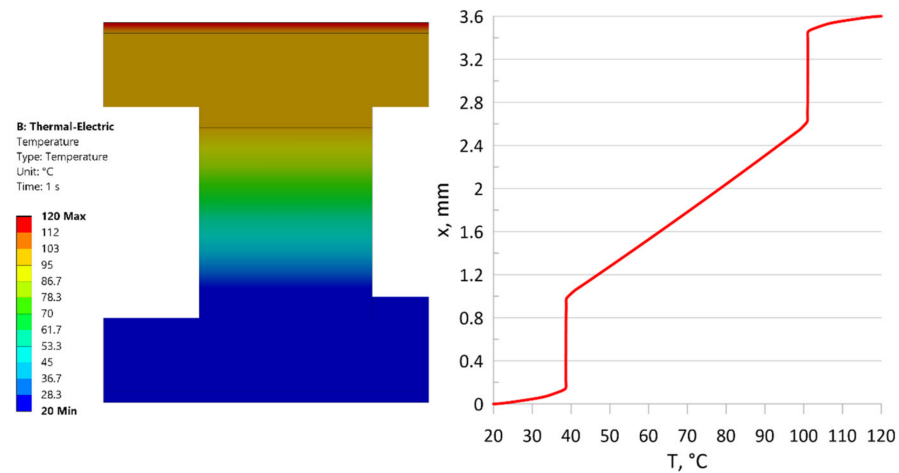


Figure 3. Temperature field in the TEG cross-section when the thermal resistance is on the hot side.

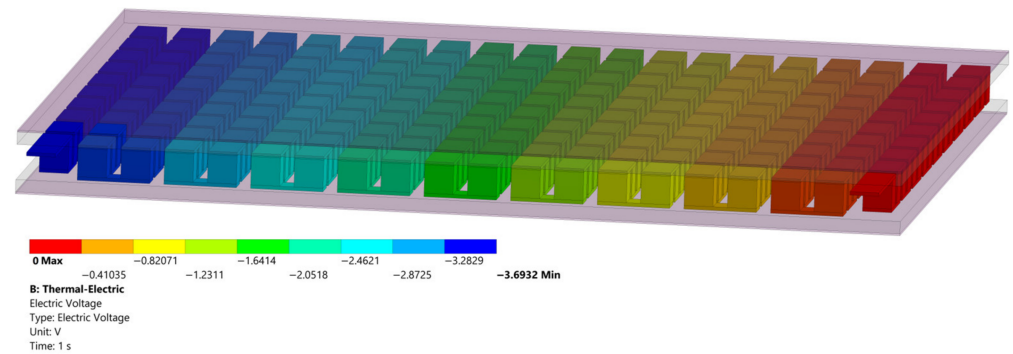


Figure 4. Voltage field on the TEG junctions.

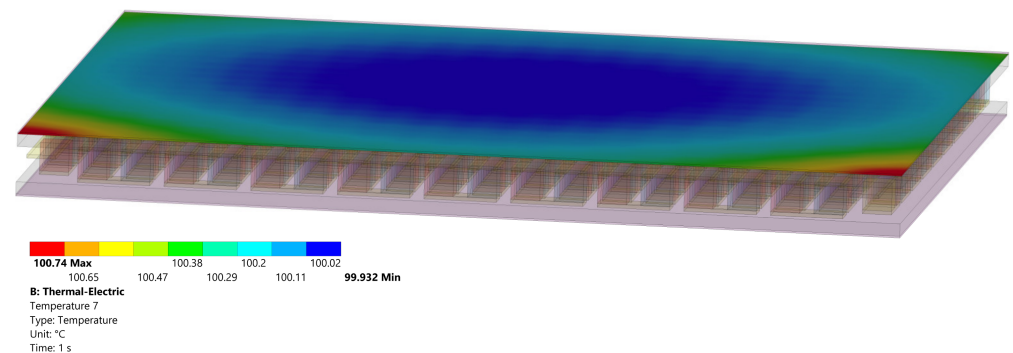


Figure 5. Temperature distribution on the hot surface of the TEG module.

The average temperature of the thermoelectric leg across the TEG is 60.4 °C. In these conditions, the voltage on the TEG terminals is 3.69 V (see Figure 4), and the generated electric power totals 8.3 W. Figure 5 shows the temperature on the TEM surface.

The temperature differs by less than 1 K, with the largest deviation at the corners where the terminals are located. By comparing the temperature variation with the temperature level, we can assume that the temperature is uniform. This, in turn, provides a good justification for the application of the 1D model.

To validate the quality of the developed software based on the 1D model, a series of tests was conducted by comparing the results with the 3D FEM model presented above. Several key operating parameters were selected for the comparison, including the maximum output power, current at maximum power, short-circuit current, heat delivered at open-circuit and short-circuit, and open-circuit voltage. These parameters were compared

for various configurations of assumed thermal resistances. The absolute relative error for each parameter was then evaluated (Table 1).

Table 1. Comparison of results obtained from the 1D and 3D models of the TEG.

$r_h/r_c, \mu\text{Km}^2/\text{W}$	Parameter	1D	3D	Absolute Error, %
220/220	P_{TEG}^{max}, W	5.85	5.84	0.2
	$I(P_{TEG}^{max}), \text{A}$	1.81	1.8	0.6
	I_{SC}, A	3.62	3.59	0.8
	$\dot{Q}_h(I=0), \text{W}$	146.26	145.13	0.8
	$\dot{Q}_h(I=I_{SC}), \text{W}$	226.65	225.22	0.6
	V_{OC}, V	6.48	6.50	0.3
0/220	P_{TEG}^{max}, W	8.4	8.38	0.2
	$I(P_{TEG}^{max}), \text{A}$	2.25	2.24	0.4
	I_{SC}, A	4.49	4.46	0.7
	$\dot{Q}_h(I=0), \text{W}$	167.76	166.37	0.8
	$\dot{Q}_h(I=I_{SC}), \text{W}$	286.32	284.61	0.6
	V_{OC}, V	7.43	7.45	0.3
220/0	P_{TEG}^{max}, W	8.33	8.31	0.2
	$I(P_{TEG}^{max}), \text{A}$	2.25	2.24	0.4
	I_{SC}, A	4.53	4.50	0.7
	$\dot{Q}_h(I=0), \text{W}$	167.76	166.37	0.8
	$\dot{Q}_h(I=I_{SC}), \text{W}$	279.05	277.40	0.6
	V_{OC}, V	7.43	7.45	0.3
0/0	P_{TEG}^{max}, W	13.03	12.99	0.3
	$I(P_{TEG}^{max}), \text{A}$	2.99	2.96	1.0
	I_{SC}, A	5.99	5.95	0.7
	$\dot{Q}_h(I=0), \text{W}$	196.66	194.91	0.9
	$\dot{Q}_h(I=I_{SC}), \text{W}$	375.55	373.22	0.6
	V_{OC}, V	8.71	8.73	0.2

We can see that the discrepancies between the models are generally below 1%, so the results confirm the considerable usefulness of the 1D model, despite its limited dimensionality. For this reason, further analyses related to the determination of the TEG characteristics are conducted using the software developed based on it. This decision results from the fact that the 1D model is characterized by very short computation times, which proves its great advantage in comparison with expensive and time-consuming FEM simulations.

4.2. Performance Comparison of the TEG

To determine the full characteristics of the investigated TEG, calculations were carried out on its current-dependent power (see Figure 6) and efficiency (see Figure 7) characteristics. Three cases were considered: 1—no contact resistance ($r_h = 0 \mu\text{Km}^2/\text{W}$, $r_c = 0 \mu\text{Km}^2/\text{W}$), 2—resistance located on the hot side ($r_h = 220 \mu\text{Km}^2/\text{W}$, $r_c = 0 \mu\text{Km}^2/\text{W}$), 3—resistance located on the cold side ($r_h = 0 \mu\text{Km}^2/\text{W}$, $r_c = 220 \mu\text{Km}^2/\text{W}$), and 4—resistance located on both sides ($r_h = 220 \mu\text{Km}^2/\text{W}$, $r_c = 220 \mu\text{Km}^2/\text{W}$). The first case corresponds to an idealized situation, while the others are the cases of inclusion of contact resistance in the model. Usually, it is assumed in the calculations that contact resistances are of the same

magnitude on both sides of the TEG module. By considering cases 2 and 3, the influence of respective side resistance on the TEG performance can be determined.

It follows from the presented charts (Figures 6 and 7) that the presence of thermal resistance on either side results in a distinct deterioration in both the maximum power and efficiency. It also decreases the short-circuit current. The location of the thermal resistance has a very slight impact on the TEG power and efficiency characteristics. From a practical standpoint, in most situations, this is therefore insignificant. It is worth noting, however, that if thermal resistance occurs on the hot side, the maximum power is 8.33 W, corresponding to a current of 2.26 A, while if it is located on the cold side, the values are 8.40 W and 2.25 A, respectively. The short-circuit currents are 4.52 A for the hot side resistance and 4.49 A for the cold side resistance. The maximum efficiency of the TEG in the two situations is 3.69% (for 1.95 A) and 3.73% (for 1.90 A), respectively. The higher efficiency corresponds to the location of the resistance on the hot side. This is because the average temperature of the junctions is lower than in the case with resistance on the cold side, which, in turn, results in a slightly lower value of the Peltier coefficient. This phenomenon decreases the heat flow, thus increasing efficiency. In Figure 6, there are also results obtained with the FEM model. There is a very good agreement with the 1D approach.

To gain a deeper understanding of the presented characteristics, an analysis of the deviation between the thermoelectric junction temperature and the temperature of the corresponding heat exchanger was conducted. The emphasis was placed on the TEG side, specifically where the contact resistance was situated. The results, depicted in Figure 8, showcase the temperature differences ($T_{ha} - T_h$) and ($T_c - T_{ca}$) as functions of the flowing current. In other words, the chart shows the deviation between heat source/sink difference and thermoelectric junction difference. The temperature deviations for the two junctions demonstrate different dynamics.

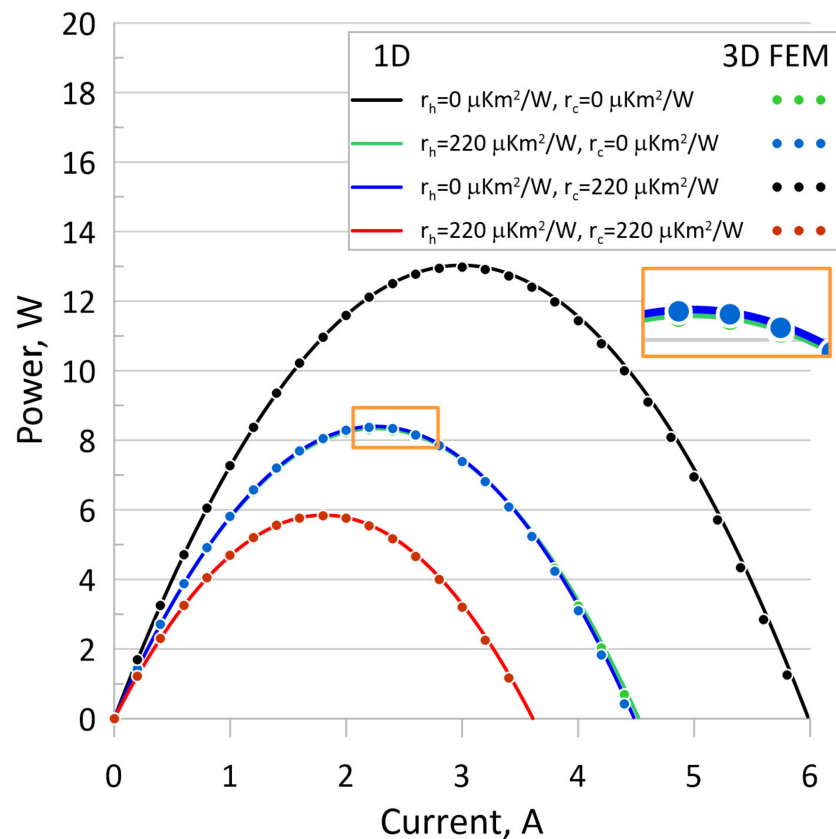


Figure 6. TEG power as a function of current for various distributions of contact resistances.

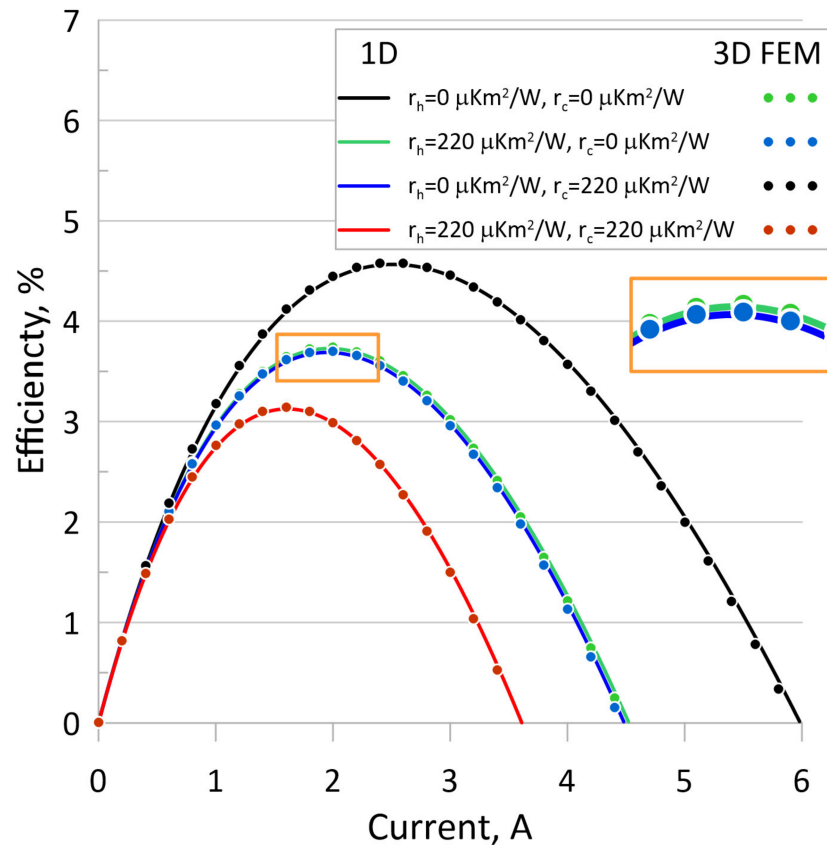


Figure 7. TEG efficiency as a function of current for various distributions of contact resistances.

The presence of thermal resistance results in an increase in temperature difference with current, as the current generates Peltier heat, leading to a greater temperature “loss” across the thermal resistance. When the thermal resistance is situated on the hot side, an increase in electric current corresponds to a drop in the rate of changes (derivative) in the junction temperature deviation. This is because an increase in current results in higher absorption of heat by the TEG, known as the Peltier effect, leading to a decrease in junction temperature. This phenomenon arises from a reduction in the Peltier coefficient caused by the temperature diminish in this scenario. Conversely, if the thermal resistance is positioned on the cold side, an elevation in the heat conducted by the resistance layer (caused by the Peltier effect) raises the temperature of the TEG’s cold side. This, in turn, amplifies the Peltier coefficient and directly intensifies the impact of temperature changes, resulting in an enlargement of temperature deviation (positive second derivative). Initially (for zero current), the rate of change (derivative) in the temperature deviation is higher in the case of r_h presence (compared with the presence of r_c) because the hot heat flow is also higher. This difference in heat flow (enlargement on the hot side) is due to the first law of thermodynamics (where some heat is converted to electricity) and becomes more significant with increasing current, up to the point where maximum power is reached. The curves presented in Figure 8 explain why for the cold-side case ($r_h = 0 \mu\text{K}m^2/\text{W}$, $r_c = 220 \mu\text{K}m^2/\text{W}$), the maximum power in Figure 6 is higher than in the opposite case, even though the short-circuit current is smaller. This observation is consistent with the efficiency difference illustrated in Figure 7.

It is worth noting that an increase in current brings about a modification in the disparity between the heat flow conducted to/from the heat exchangers. This stems from the transfer of a portion of energy to the external environment in the form of electricity within the analysed system.

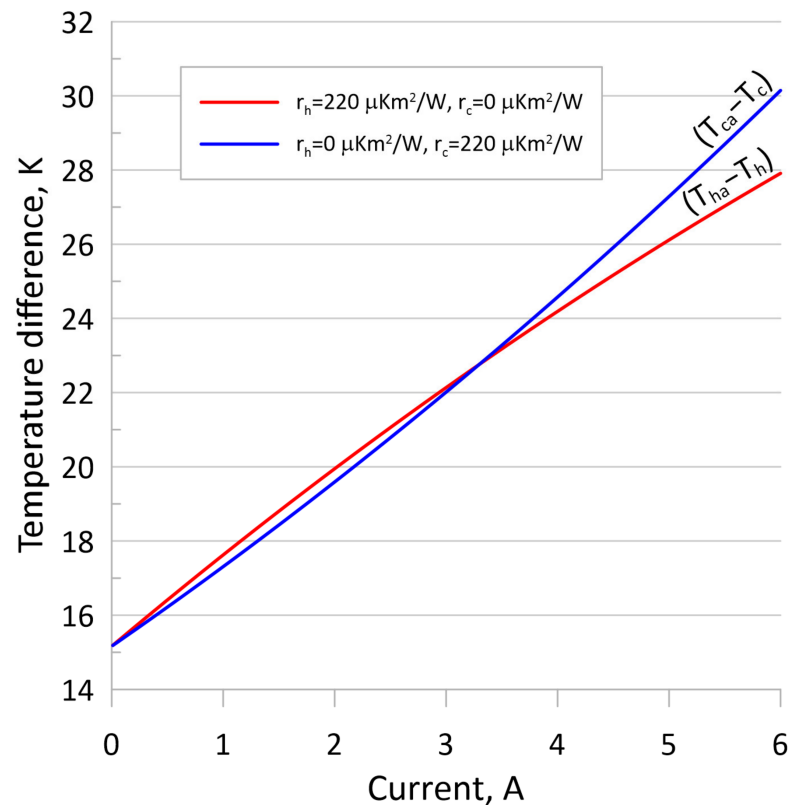


Figure 8. Deviation in the thermoelectric junction temperature from the temperature of the corresponding heat exchanger as a function of current in the TEG.

4.3. Influence of Heat Source Temperature

In the next step, it was decided to investigate how contact resistance affects the operating parameters of the TEG system with changing values of the upper heat source temperature. For this purpose, a constant temperature was set for the heat sink at 20 °C, and the temperature of the heat source was gradually increased for analogous cases of thermal contact resistance occurrence. The increase in the temperature T_h would result in an increase in the effective temperature difference across the thermoelectric junctions, and consequently, an increase in the system's power. The change in power is a nonlinear function of the heat source temperature, as indicated by Equation (10). The negative impact on the increase in the temperature difference across the junctions will be caused by the presence of thermal resistances between the heat source/sink and the thermoelectric junctions, which occur in almost all terms of Equation (10). We can infer that thermal resistance will limit efficiency based on the deterioration in heat flow through the module. However, it is challenging to discern the nature of the impact of these resistances based on the mentioned equation.

Analysing the obtained results, we can observe that the maximum values of power and efficiency do indeed increase with the rising temperature difference between the heat source and heat sink, and the nature of their growth is nonlinear. However, the maximum power of the system is characterized by significantly greater nonlinearity. The rate of growth for both quantities is mainly determined by the total thermal resistance of the heat flow between the heat exchangers, with the location of this resistance playing a marginal role. In the case of power (Figure 9), the difference in its values is practically imperceptible, whether the resistance occurs on the cold or hot side of the module. A slightly higher value for the 0/220 resistance configuration than for 220/0 is observed because the heat is smaller on the cold side. However, slightly larger differences, albeit still practically insignificant, are noted in the case of efficiency (Figure 10). The greater value corresponds to the 220/0 case when the thermal resistance is placed on the hot side. In this scenario, there is a lower

average temperature of joints, leading to a lower Peltier coefficient. Consequently, the heat conducted through the thermal resistance layers is smaller on average, resulting in a reduced temperature gradient on the thermal resistance and, as a consequence, a greater useful temperature difference at the thermoelectric joints.

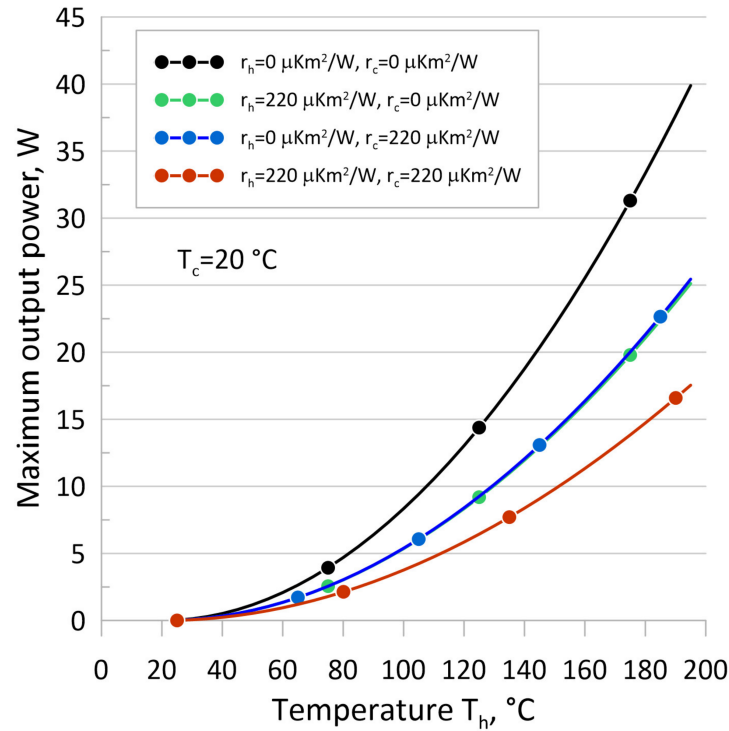


Figure 9. TEG maximum output power vs. temperature of the heat source for various distributions of contact resistances.

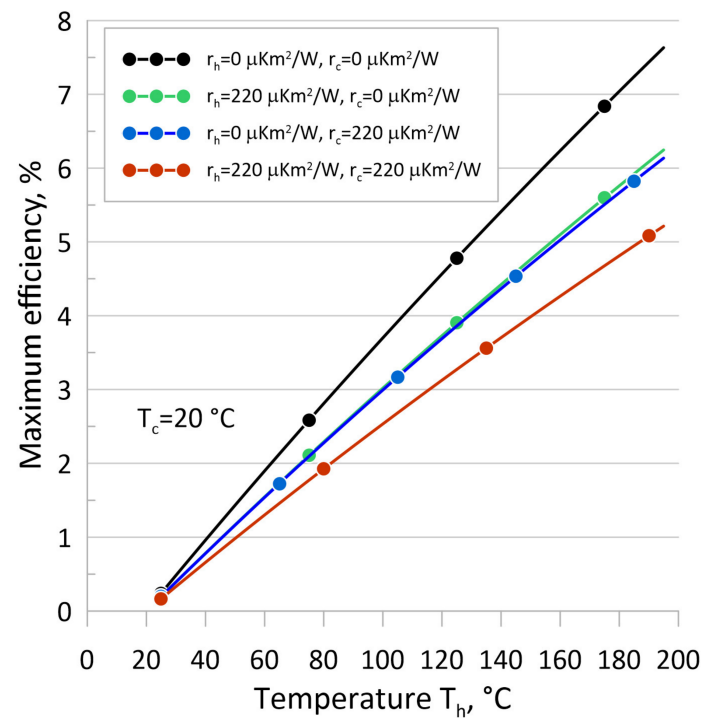


Figure 10. TEG maximum efficiency vs. temperature of the heat source for various distributions of contact resistances.

The depicted curves have a negative second derivative. This is due to the fact that for a larger temperature difference, the electric current values corresponding to maximum power or maximum efficiency are larger. Therefore, despite heat conduction following Fourier's law, there is a significant increase in Peltier heat due to higher current and higher temperature of joints. These phenomena contribute to an enhanced heat transfer between the heat source and sink. Nevertheless, completely neglecting the contact resistance leads to a significant overestimation of both indicators of the TEG's performance.

4.4. Influence of Average Temperature

To determine the effect of the TEG average temperature on its characteristics, simulations were performed for higher heat source/sink temperatures (220 °C and 120 °C). It should be emphasized here that this temperature range is higher than the allowable limit for the module in question, and the only purpose of such calculations is to clearly illustrate the influence of the average temperature on the characteristics of the TEG. The exchanger temperature difference is the same (100 K) in both cases (120 °C/20 °C and 220 °C/120 °C). The other parameters of the thermoelectric generator, including the contact resistance value, also remain unchanged. Figures 11 and 12 present a comparison of the TEG characteristics for the temperatures of 120 °C/120 °C and 220 °C/120 °C. The two cases differ only in the TEG average temperature. The results illustrate the cases when the whole contact resistance occurs on the module one side only—hot or cold.

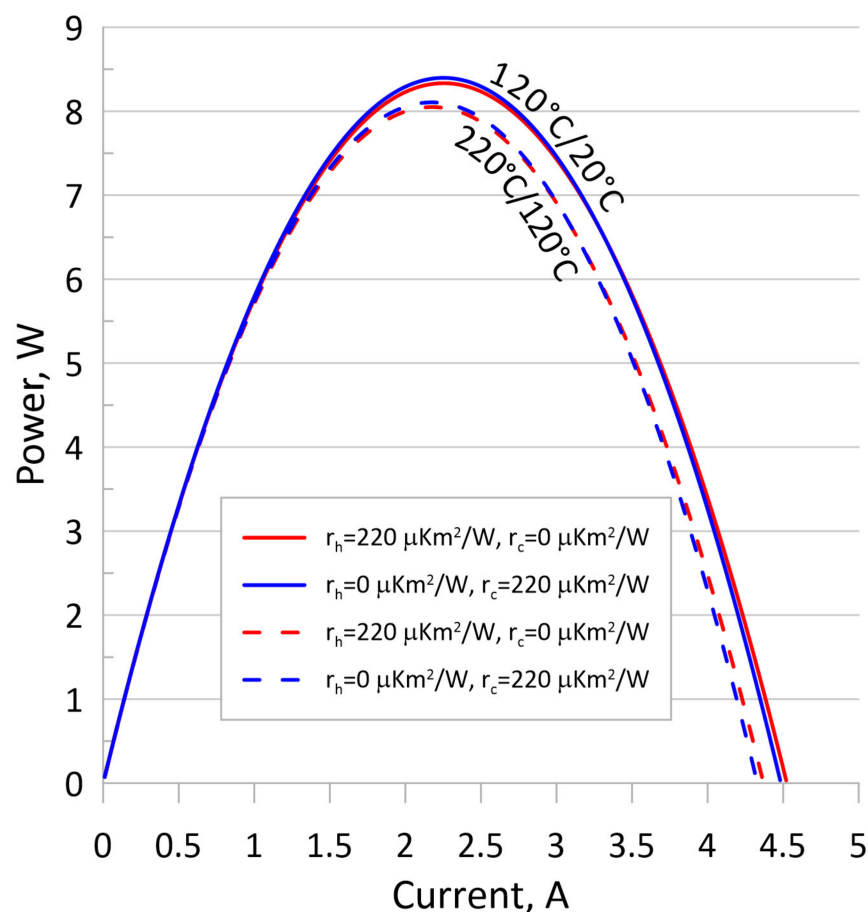


Figure 11. Curves illustrating the influence of temperature on TEG power.

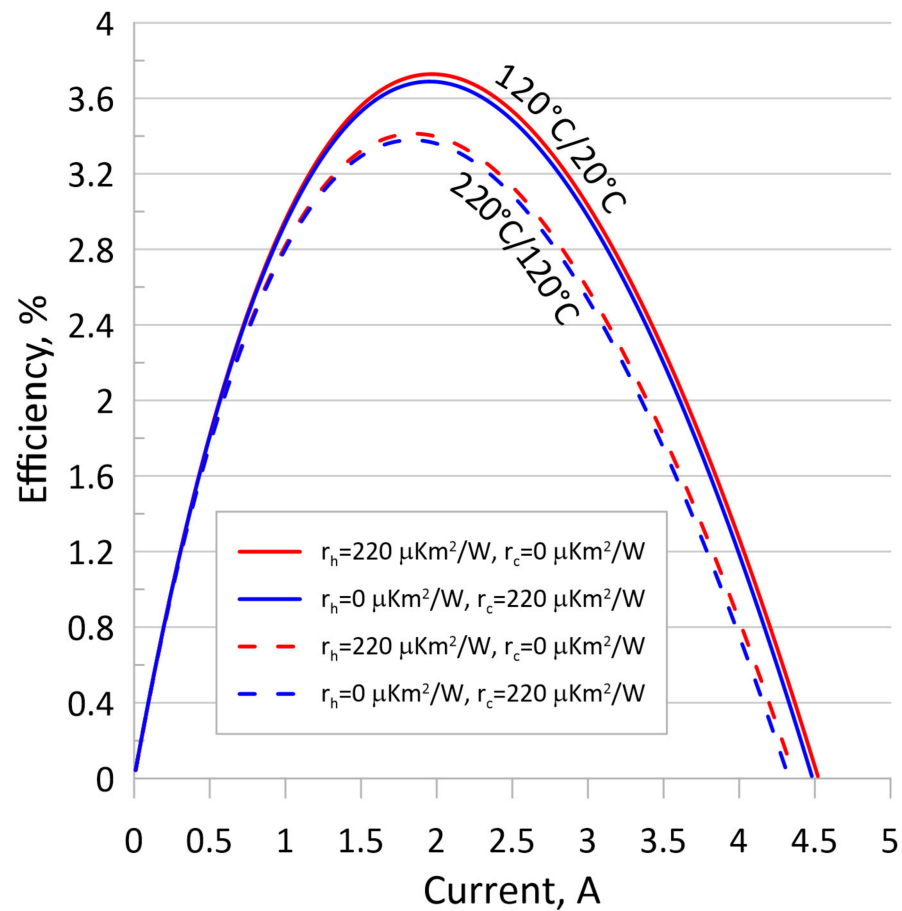


Figure 12. Curves illustrating the influence of temperature on TEG efficiency.

For the higher temperature range of the exchangers, the voltage generated by the TEG, in the absence of the current flow in the circuit, is the same as in the case of lower temperatures (which is due to the identical temperature difference). The same is true for temperature “lost” in the two thermal resistance contact layers. The differences become apparent when current flows through the TEG, and they result directly from the value of the Peltier coefficient. Because the coefficient is linearly dependent on the absolute temperature, the observed impact of the Peltier effect is stronger for higher temperatures of the TEG junctions. It can be clearly seen that the curves that illustrate the characteristics of TEGs lose their parabolic character with increasing temperature. This is due, among others, to the increasing influence of the factor related to I^3 (Equation (10)). The electrical current corresponding to the points of maximum power and efficiency decreases, and, importantly, changes to a greater extent than the value of the short-circuit current. However, as in the situation described above and despite the significant deformation of the characteristic curves, the effect of on which side the thermal resistance is located appears to be relatively small. The curve describing the parameters for the higher average temperature is characterized by greater symmetry. This is due to the smaller variation in Peltier heat, which is directly related to temperature. The changes in temperature degradation related to the thermal resistance of the system are proportional to the heat flow. However, their relative changes (with respect to 0 K) are smaller for the case with a higher mean temperature. The same observation applies to the variation in Peltier heat. This explains the differences in curve symmetry.

4.5. Impact of the Leg Height of the TEG

Next, an analysis of the impact of the height of the TEG legs on the thermoelectric generator performance was conducted. The values of the *EMF* generated by the TEG in

the open circuit for the temperatures of the heat source and heat sink of 120 °C/20 °C depending on the height of the legs are shown in Figure 13.

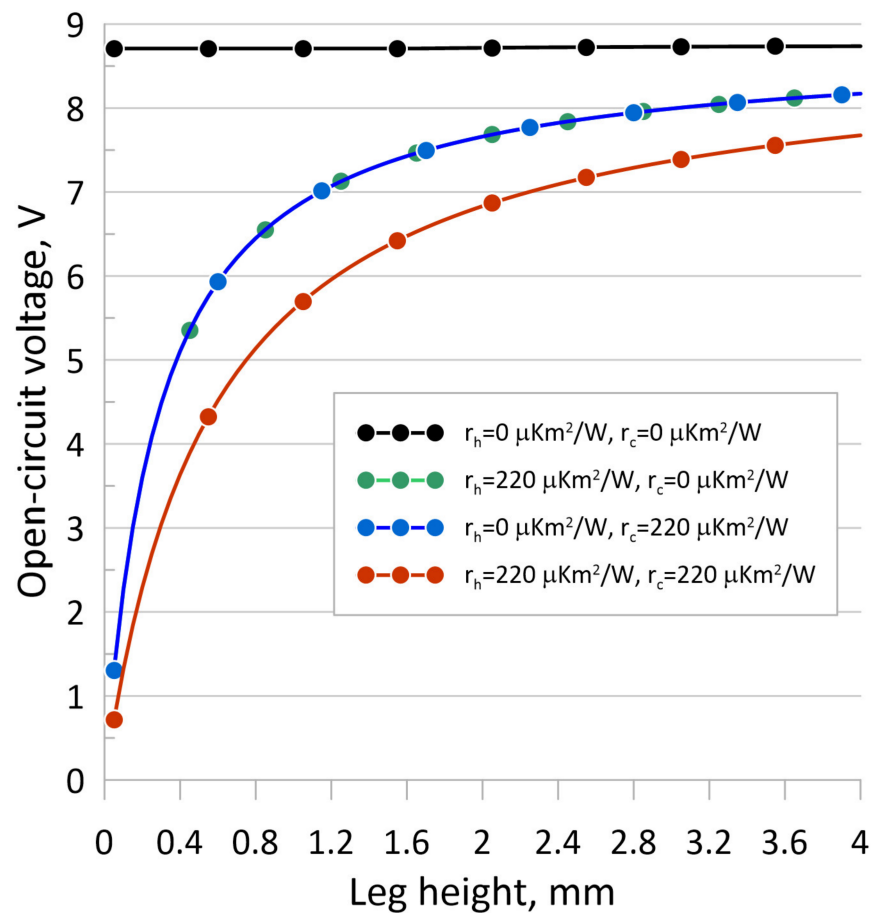


Figure 13. TEG open-circuit voltage depending on the leg height for various distributions of contact resistance.

The curves presented in Figure 13 primarily reflect the impact of the distribution and magnitude of thermal resistances on the temperature distribution within the system. When the legs are very short, their thermal resistance is minimal, causing the contact layers to bear most of the thermal resistance between the heat source and the heat sink. Consequently, this results in a marginal difference in junction temperatures and a consequently low voltage. As the height of the legs increases, the contribution of the TEG thermal resistance to the total resistance also rises, leading to an increased temperature gradient across the thermoelectric junction and consequently, a higher voltage. The analysis indicates that the voltage asymptotically approaches the value corresponding to zero contact resistance. However, it is crucial to note that an elevation in leg height entails a growth in the overall thermal resistance of the system, causing a reduction in the heat transferred via the TEG. Additionally, electrical resistance also increases, resulting in lower output power and a decreased short-circuit current. In Figure 13, it is noteworthy that the distribution of contact resistance becomes inconsequential, as the curves coincide in both extreme cases (where the entire resistance is located on one side—either hot or cold). This uniformity arises due to the absence of thermoelectric phenomena influencing heat flow ($I = 0$). Also, it should be noted that in the case of $r_h = r_c = 0$ (zero contact resistance), the heat flow tends to infinity as the leg height tends to zero (infinite heat low).

In the case of the value of the short-circuit current as a function of the leg height, the situation looks different, as presented in Figure 14.

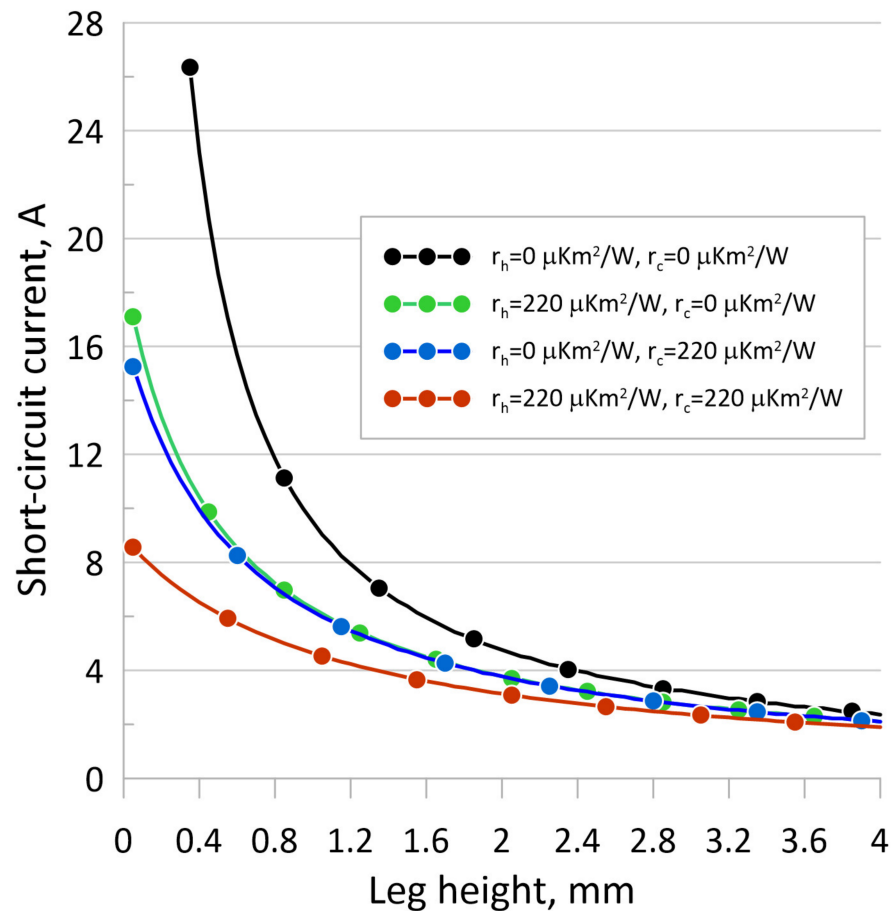


Figure 14. Short-circuit current depending on leg height for various distributions of contact resistance.

In this context, the discernible difference in short-circuit current values for various contact resistance distributions becomes apparent. These variations are most pronounced with shorter legs and diminish as the leg height increases. In a short-circuit state, the heat released and absorbed by the TEG are equal since the disparity in heat generated by different Peltier coefficients (temperature variability) is offset by Joule heat. The distinct short-circuit current values arise from the diverse temperature gradients across the junctions, a consequence of varying Peltier coefficients.

When thermal resistance is situated on the hot side, the average temperature of each junction is lower compared with the scenario where thermal resistance is on the cold side. A higher Peltier coefficient, resulting from elevated temperature, leads to a more substantial increase in heat flow per ampere. Consequently, this causes a greater temperature deviation—the temperature “lost” in thermal resistance layers. This phenomenon results in a reduced effective gradient when a non-zero current is applied. This explains the non-uniformity observed between the two middle curves in Figure 14 and subsequent calculations.

Figure 15 shows the curves illustrating changes in the TEG maximum power depending on leg height.

Similar to in the case of the sc current (and for the same reasons), the effect of the contact resistance location is noticeable, especially for very short legs. As the leg height increases beyond the point of maximum power, the differences in power diminish, two curves cross each other, and the attained values approach the scenario where contact resistances are absent. Conversely, when examining the maximum efficiency of the TEG (Figure 16), a slightly higher efficiency is observed when the resistance is located on the hot side of the thermoelectric generator. This observation aligns with the explanation provided earlier for the short-circuit current (lower Peltier coefficient due to the lower

temperature). The maximum efficiency, similar to power, is close to the efficiency of a system with no contact resistance for a large leg height. In this case, it is slightly above 4.5%. The relative difference between the values (both efficiency and power) for various cases of thermal resistance placement is most significant near the leg height corresponding to the maximum power.

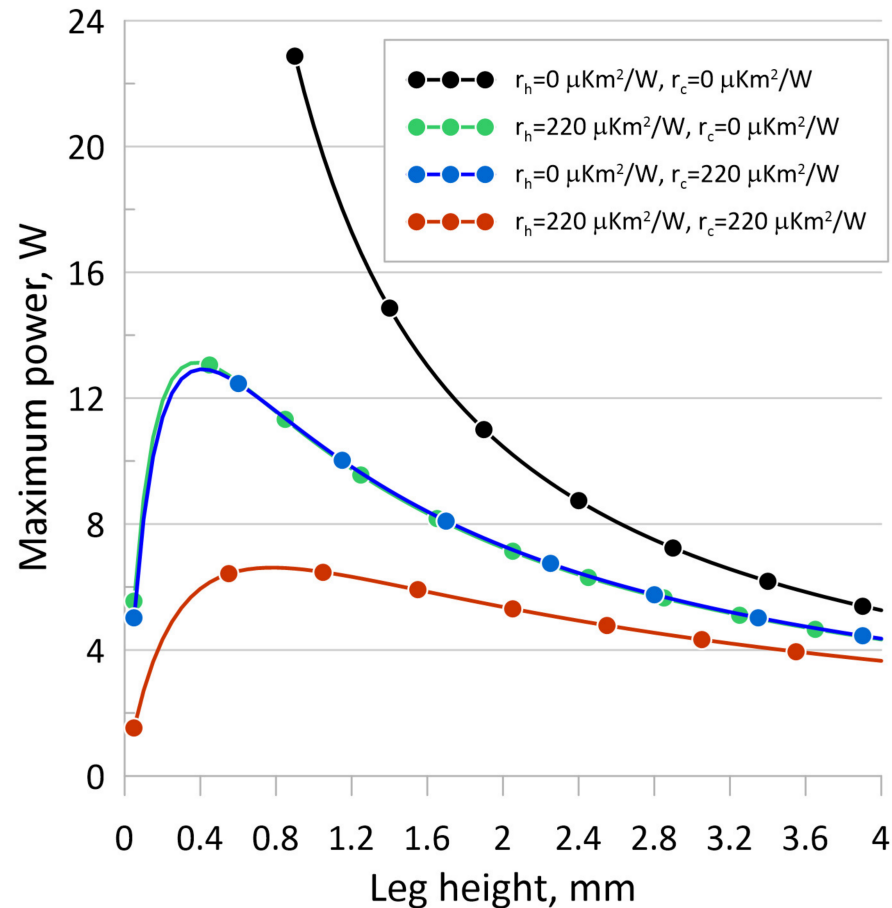


Figure 15. Maximum TEG power depending on leg height for various distributions of contact thermal resistance.

4.6. Operation in the Heat Pump Mode—Refrigerator Application

In the case of a cooling mode operation, the thermoelectric cooler (TEC) is supplied with electric power to drive the heat flow against the thermal gradient. Here, the range of operation temperature is generally lower, and the aim of such a device is to cool a given space (i.e., refrigerator) or component (i.e., electronic element). Although the general observations gained for the TEG are also valid for the TEC, some additional research concerning the heat exchange with the surroundings revealed some new insight into the thermal contact resistance influence on TEC performance. The intensity of heat exchange depends on the TEC application, which determines the needed cooling power and cooling temperature.

All the results shown below are obtained for the same thermoelectric module as described above with the applied heat resistance layers, and all analyses were performed with the same 1D model approach. The calculations were also validated using the 3D FEM model, and the discrepancies in the results were similar to those observed in the TEG validation (Table 1). However, instead of the constant temperature condition on the external boundaries, the convective heat transfer condition was applied, whose aim is to simulate, on the one side, the cooling heat, and on the other side, the heat release to the environment. In this case, the heat transfer coefficient is recalculated to a heat transfer factor (*HTF*), which represents the magnitude of heat exchanged per 1K temperature difference. On the

heat release side, the constant $HTF_h = 10 \text{ W/K}$ is set, which reflects a forced convection high-quality typical server CPU radiator. On the cooled side, the HTF_c is changed to adjust to a specific TEC application. HTF_c can reflect a cooling chamber thermal insulation or a cooling radiator, depending on its value. The ambient temperature was set to a constant of $22 \text{ }^\circ\text{C}$.

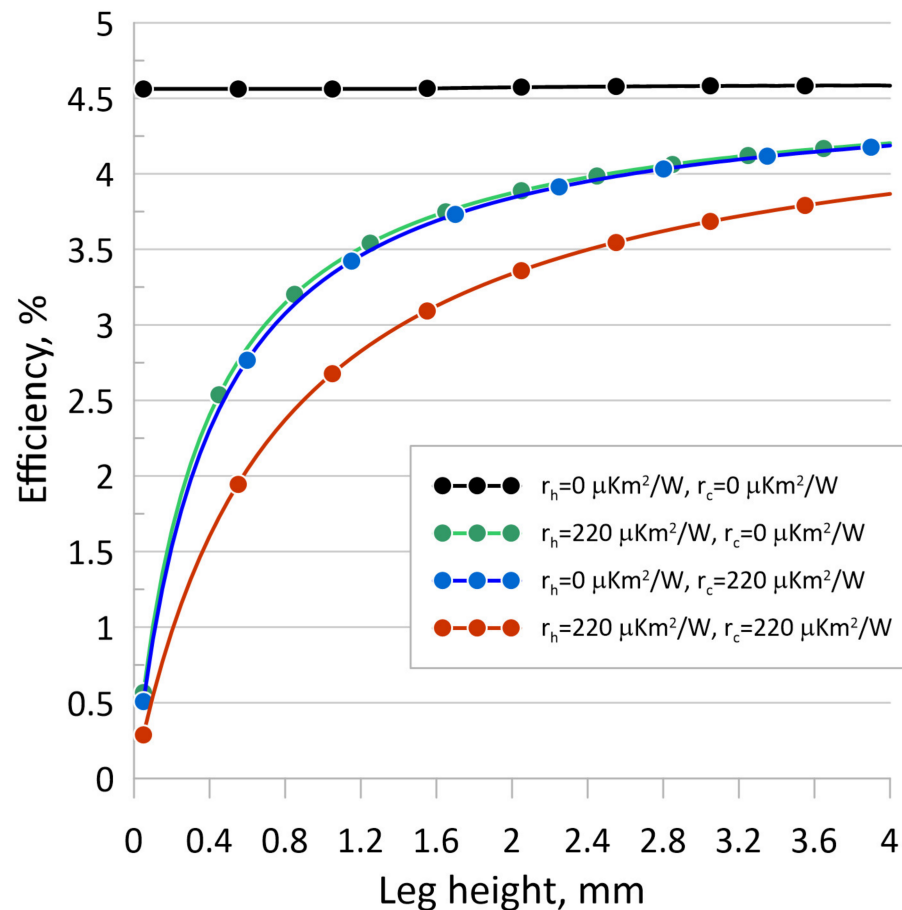


Figure 16. TEG efficiency depending on leg height for various distributions of contact resistance.

At first, the influence of the contact heat resistance on the minimum cooling temperature, supply power, and coefficient of performance (COP) was analysed for a nearly perfectly insulated cooling space with $HTF_c = 0.01 \text{ W/K}$. In this case, the temperature corresponds to the adiabatic one for the thermoelectric module in the given conditions.

In each of the above graphs (Figures 17–19), two pairs of overlapping curves can be observed. This is due to the fact that in the presented configuration, there is a low HTF_c at the cooling space, meaning it is almost perfectly thermally insulated. The temperature achieved in the steady state is practically identical to the adiabatic temperature of the cold part of the cell. Firstly, this implies that the heat supplied to the cooling space, and subsequently, to its surroundings, is negligible. Consequently, there is nearly no heat flow through the thermal resistance on the cold side, and, therefore, there is no temperature gradient/difference there related to the existence of r_c . Secondly, the temperature in the cooled space is determined solely by the electric supply conditions and the established temperature of the hot end of the system (the radiator releasing heat to the surroundings, for which $HTF_L = 10 \text{ W/K}$). Under adiabatic conditions on the cold side, the boundary temperature results from the balance of Peltier heat, Joule heat, and heat conducted through the module. Hence, the temperature on the hot side of the module plays a significant role here, which, in turn, depends significantly on the heat released to the surroundings.

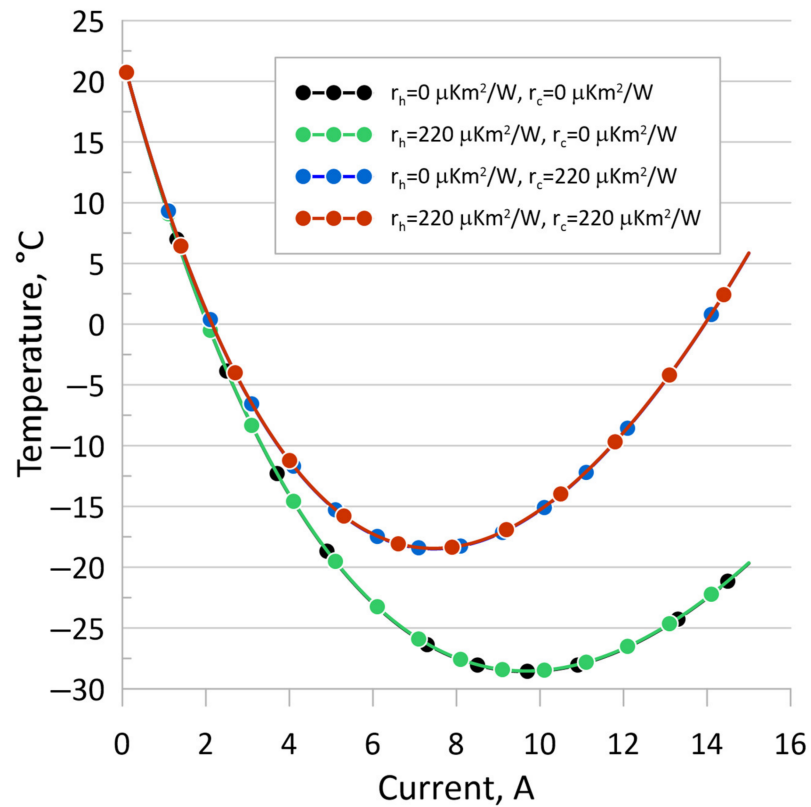


Figure 17. Temperature of cooled space in the steady state as a function of supply current for various distributions of contact resistance.

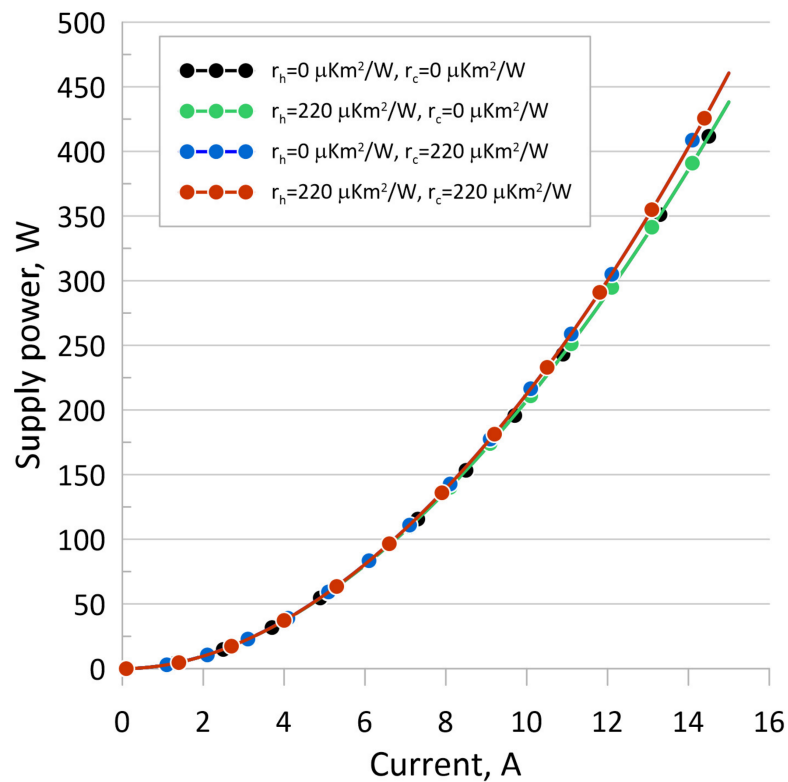


Figure 18. TEC supply power as a function of supply current for various distributions of contact resistance.

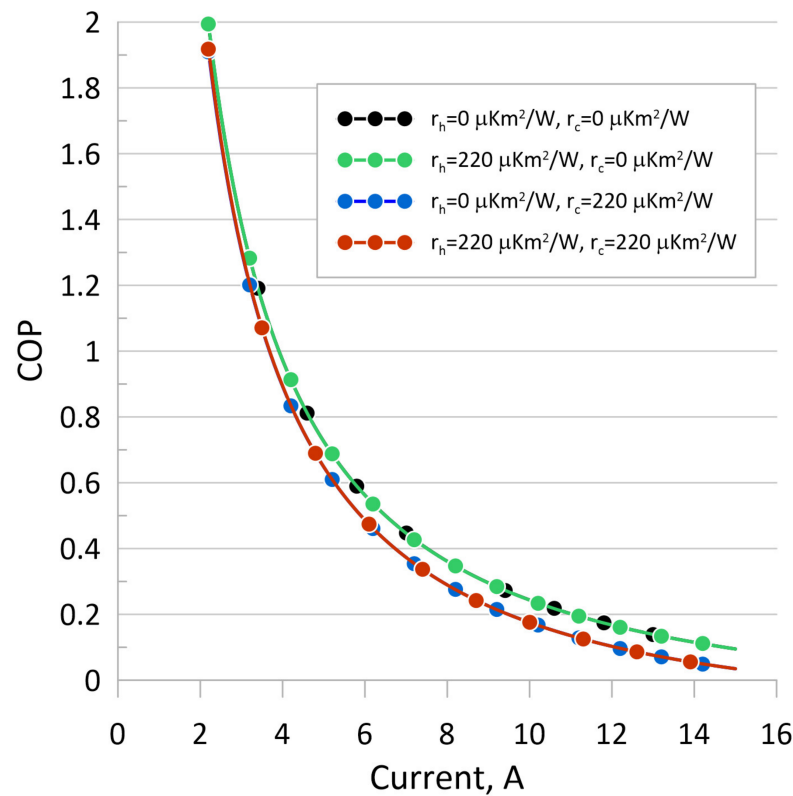


Figure 19. TEC COP as a function of supply current for various distributions of contact resistance.

The existence of thermal resistance on the hot side has a significant impact on deteriorating the cooling capacity of the device. The heat released to the surroundings due to the limited COP of the device is substantial. In practice, it is the sum of the heat absorbed from the cooled chamber (negligibly small in this case) and the supplied electrical power, which directly results from the energy balance. The supplied electrical power primarily constitutes Joule heat due to the electrical resistance of the module, with a smaller part consisting of the difference in Peltier heat on both sides of the thermoelectric legs. The significant heat released to the surroundings causes the presence of thermal resistance on the hot side to substantially increase the temperature of the hot junctions of the thermoelectric elements. This, in turn, raises the operating temperature on both sides of the module, including the temperature of the cooled space, ultimately reducing the cooling ability.

For a better illustration of the impact of individual contact resistances on the operation of the TEC, the differences in the minimum temperature obtained by the system without resistances and with their presence in various configurations are shown in the subsequent plots. Curves “1” represent the current corresponding to the maximum cooling power for a given HTF_c and operating state with specific thermal resistances (see legends). Curves “2” are curves corresponding to the maximum cooling power for the reference state, without thermal resistances.

The presented findings (Figures 20–22) reveal that the thermal resistance between the hot thermoelectric junctions and the heat sink has a significantly greater effect on the resulting temperature in the cooled space. This is attributed to a much larger heat flow on this side. In contrast, the thermal resistance between the cold thermoelectric junction and the cooled space has a negligible impact at very low HTF_c due to nearly no heat flow in the steady state. The influence of this resistance (r_c) becomes more pronounced as HTF_c increases, owing to the heightened heat flow on the cooled side. Even for the largest HTF_c shown, the impact of r_c remains moderate compared with the impact of r_h . Therefore, when utilizing a thermoelectric cooler as a refrigerator, it appears crucial to restrict the contact resistance on the heat sink side. Conversely, if the TEC were used, for instance, to cool elements generating significant heat, the thermal resistance on both sides plays

a role, although r_h has a much more significant impact. In Figure 21, for $HTF_c = 0$, the shown difference must be equal to zero, as evident in the graph, because at that point, the cooling heat flow is practically zero. This difference increases with higher current and larger HTF_c , especially for its relatively small values. For large HTF_c values, in Figures 20–22, temperature deviation decreases with increasing HTF_c . This is due to the strong dissipation of cooling heat to the surroundings, resulting in a small temperature difference between the cooling and ambient temperatures in every analysed configuration. In such cases, it would be more meaningful to analyse not the temperature but the cooling heat; in this scenario, the influence of the presence of r_h or r_c would be more significant.

For the situation where r_h exists, its impact is visible regardless of HTF_c and non-zero current. This is because the temperature at the hot end of the cell increases, leading to an increase in the temperature of the cold end and the cooled space. For small current values, the maximum deviation shown in Figures 20 and 22 corresponds to HTF_c values around 1.0.

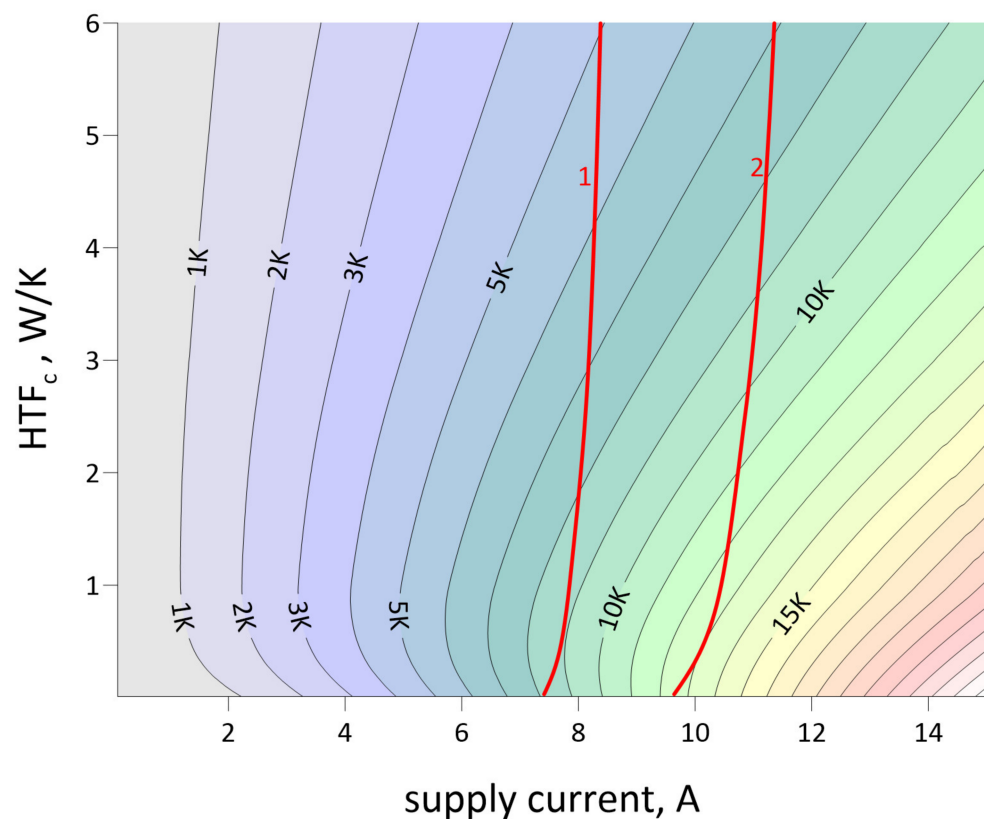


Figure 20. Temperature “loss” due to $r_h = 220 \text{ Wm}^2/\text{K}$ and $r_c = 220 \text{ Wm}^2/\text{K}$ compared to the zero-thermal resistance case for various HTF_c values and supply currents. Red lines represent electric current for maximum cooling power: 1—with r_h and r_c involved, 2—without r_h and r_c .

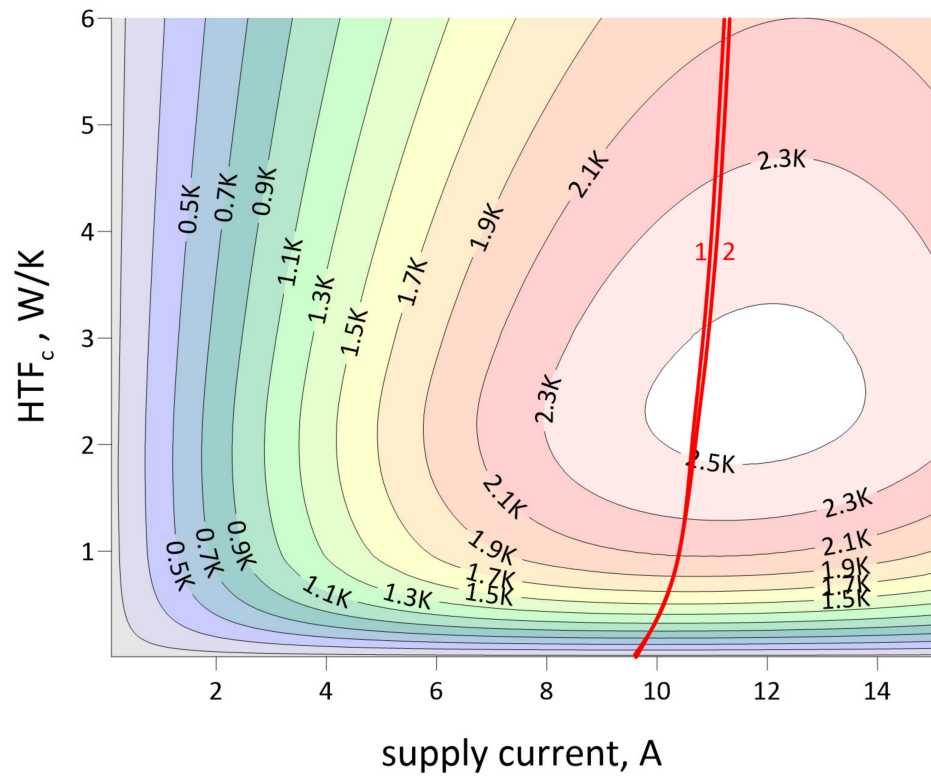


Figure 21. Temperature “loss” due to $r_c = 220 \text{ Wm}^2/\text{K}$ compared to the zero-thermal resistance case for various HTF_c values and supply currents. Red lines represent electric current for maximum cooling power: 1—with r_c involved, 2—without r_c .

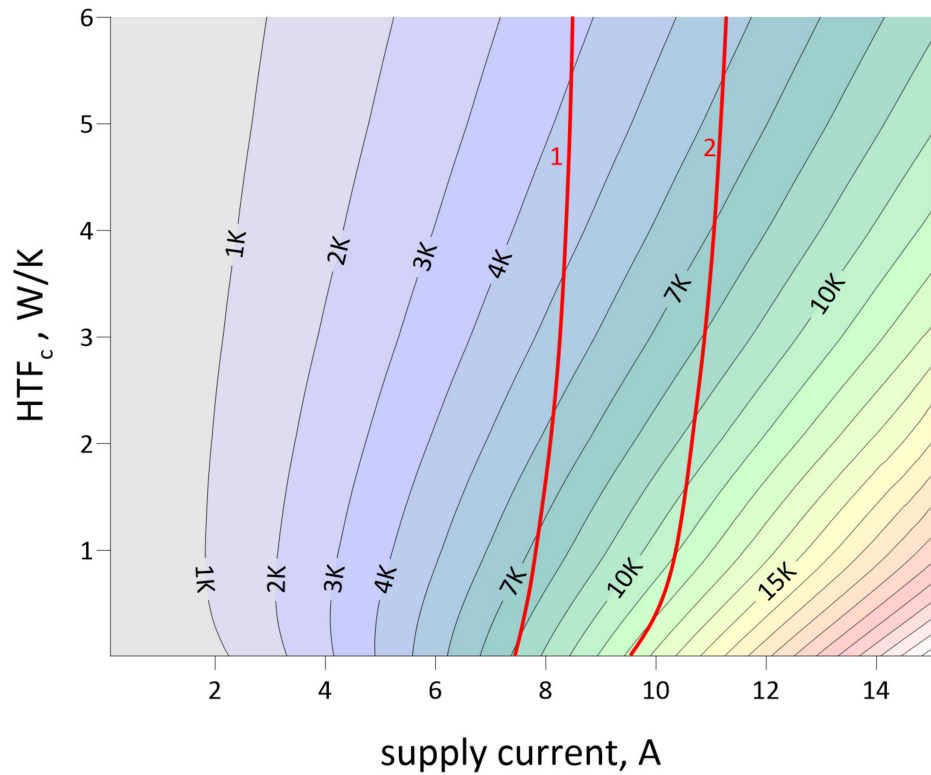


Figure 22. Temperature “loss” due to $r_h = 220 \text{ Wm}^2/\text{K}$ compared to the zero-thermal resistance case for various HTF_c values and supply currents. Red lines represent electric current for maximum cooling power: 1—with r_h involved, 2—without r_h .

5. Model Validation

The analytical model developed was validated using measurements performed on a specialist test stand. A detailed description of the stand can be found in [36]. The measuring stand is programmed to maintain the set temperature difference between the TEG heat exchangers. Two identical MULTICOMP PRO MCTE1-19913L-S supplied by Farnell UK, were tested. First, the basic operating parameters of the two modules of the same series (TEG1 and TEG2) were determined: the maximum power output, the short-circuit current, and the open-circuit voltage at a 100 K temperature difference (120 °C/20 °C) and the clamping force of 200 N. These results are shown as a “single module” in Table 2. Then, the TEGs were placed on each other (thermally connected in series) in between the heat exchangers so that one of them would simulate the deterioration in the thermal contact conditions on the surface of the other. TEG1 was in contact with the heat sink, while TEG2 was in contact with the heat source. To improve the thermal conductivity of the contact layer, thermal grease was additionally applied to the surface of the modules. The thermal resistance was measured with the rapid method [36] and gave the result of 220 $\mu\text{Km}^2/\text{W}$ for layers between the module and heat exchangers. At each test, one of the modules was the subject of investigation, while the second one was working as thermal resistance. The resistance generated by the second module depends on its operating conditions and varies with changes in current. There were two states of the “resistance module”: open circuit and short circuit conditions, which, based on the “single module” measurements from Table 2 supplemented with heat flows, resulted in a very high thermal resistance of about 1060 $\mu\text{Km}^2/\text{W}$ and 1600 $\mu\text{Km}^2/\text{W}$, respectively. A comparison between model results and measurements for the “double module” configuration shows a good agreement with less than 15% relative error. In the next part of the tests, the measured TEGs were swapped. In general, the thermal resistance of a TEG with a connected resistor that allows current flow decreases with a rise in current (up to the short-circuit state). This is due to the Peltier effect. Measurements were made when the temperatures of both exchangers reached a steady state. The measurement accuracy was 0.01 V and 0.01 A, and the temperature was kept within the limit of ± 0.5 °C. The results of the measurements are listed in Table 2 for open-circuit voltage (V_{oc}), short-circuit current (I_{sc}), and maximum power (P_{max}).

Table 2. Measured TEG parameters.

		TEG1	TEG2	
single module	V_{oc} , V	6.52	6.23	
	I_{sc} , A	3.62	3.54	
	P_{max} , W	5.91	5.51	
resistance module at short circuit	V_{oc} , V	4.01	3.95	
	I_{sc} , A	1.78	1.9	
	P_{max} , W	1.82	1.88	
double module	resistance module at open circuit	V_{oc} , V	3.35	3.20
	I_{sc} , A	1.42	1.48	
	P_{max} , W	1.21	1.19	

The data gathered in Table 2 indicate that the tested TEGs were not identical. However, it is very hard to determine the reasons for such an observation; this is probably due to manufacturing non-uniformity. The manufacturer’s datasheet indicates, for example, that the TEM internal electrical resistance may vary within $\pm 10\%$. Both modules were brand new and had not been used before. The parameters of TEG1 are slightly lower, but the calculated value of the internal electrical resistance is almost the same in both cases. The achievable power of the TEGs differs by less than 8% for the single investigated module.

If only one thermoelectric generator (TEG1 or TEG2) is tested in the sandwich configuration and the other is used as an additional thermal resistance in the short-circuit state, the power output of the generators are 1.82 W and 1.88 W. In the same case, but with the other TEG in the open-circuit state, the powers are 1.42 W and 1.48 W, respectively. We can observe that an increase in total contact resistance leads to an obvious drop in power. The measurement results confirm the conclusion obtained with the analytical model, i.e., that the location of contact resistance is not very significant, but the key factor is the magnitude of the total resistance. It can also be observed that an increase in additional resistance on the cold side (no “resistance” TEG → “resistance” TEG in the sc state → “resistance” TEG in the oc state) has a stronger impact on the operating parameters of the TEG, which also confirms the modelling results. Simulations carried out for the high thermal resistance generated by the “resistance TEG” yielded consistent results with the experimental data.

6. Discussion of Results

The calculations carried out using the developed model of the TEG system enable an analysis of the effect of the presence and distribution of the contact resistance on both sides of the thermoelectric module on the achieved performance of the TEM system. It can be concluded from the calculation results that the maximum power and the maximum efficiency of energy conversion depend substantially on the magnitude of contact resistance. The same can be applied to cooling temperature in the TEC system. Two extreme cases of contact resistance location were investigated: on the hot side only, on the cold side only, and on both sides. An ideal situation—zero contact resistance was also shown for comparison purposes. The calculation results indicate that, at a considerable difference in contact resistance between the hot and the cold side, the change observed in the TEG short-circuit current is slight. Differences in maximum power and efficiency are also negligible and seem to have no practical significance in most cases. The results were obtained for legs with a height of 1.5 mm, which directly corresponds to the investigated commercial TEM. Analyses were also conducted on the impact of leg height, which changes the thermal and electrical resistance inside the TEG, on its performance. In the absence of contact resistance, the TEG power approaches infinity if the leg height approaches zero. This is because in this case, the generated voltage is constant (the temperature difference responsible for this voltage is directly the difference between the heat source and the heat sink). The heat flux then increases because the thermal resistance of the legs decreases, and when the leg height approaches zero, the heat flow tends to infinity (assumed constant temperature of the ideal heat source/sink). For a very short leg, very small internal electrical resistance also occurs, which causes the short-circuit current asymptotic increase to infinity. The effect of the presence of contact resistance, however distributed, is that both power and current take on finite values. In practice, as leg height decreases, the percentage share of contact resistance in the total thermal resistance between exchangers increases. This makes it necessary, even for very small contact resistances, to consider them in the analysis of the TEG operation. It can be clearly seen that at a set value of contact resistance, leg height can be selected so that TEG power can reach its maximum. For optimal leg height, the TEG thermal resistance is sufficient to induce an adequate temperature difference at the thermoelectric junctions. At the point of maximum power, a relatively small height of the leg ensures the flow of a sufficiently large heat (which decreases monotonically with an increase in leg height) with low electrical resistance. Electrical resistance is the second parameter, after thermal resistance, that affects the system power (the third is the Seebeck coefficient). The maximum efficiency increases monotonically, which is due to the increase in the temperature gradient on the junction and the parallel decrease in the heat flux transferred between the heat source and heat sink.

The obtained research results indicate that neglecting the thermal contact resistances during the analysis of thermoelectric system performance significantly alters the obtained parameters, causing the system’s performance indicators to reach overly optimistic values. In the case of TEG, the location of the resistance has less significance, and rather, its total

value from both sides of the module matters. This is because the heat flows on both sides are similar—due to a low conversion efficiency of energy, only a small part is converted into electricity. For resistance occurring only on the hot side, the temperatures of thermoelectric junctions are lower than in the case of resistances only on the cold side, resulting in a lower Peltier coefficient and a smaller heat increase with current rise. On the other hand, the heat flow through the hot side thermal resistance is slightly bigger, causing this layer to be more important. However, the difference in the module's useful parameters is marginal and has no practical significance for the same magnitude of the thermal resistance and a different placement.

However, the situation looks different in the case of the TEC. The impact of the resistance on the hot side (heat release to the surroundings) is always relatively significant. It becomes greater as more heat is absorbed on the cooled side (higher temperature at the cooled end of the module), which directly follows from the first law of thermodynamics. The influence of the resistance on the cold side strongly depends on the system's operational conditions. When maintaining a low temperature on this side (e.g., close to adiabatic), meaning a low heat flow, the effect of the resistance on this side is very small. This impact increases with the higher heat release, i.e., when the temperature at the cold end of the module is higher despite significant cooling power (e.g., operating as an air conditioner).

7. Conclusions

The simulations performed based on the developed analytical model concern the modelling of the operating parameters of a thermoelectric module with different distributions of thermal resistances in the system. The constructed model makes it possible to take account of the differences in contact resistance on both sides of the thermoelectric module. It should be noted here that in the case of equal resistances on both sides of the module, Equation (7) becomes linear with respect to the current, which enables the direct determination of the explicit form of the short-circuit current and power.

The problem is more effectively and flexibly addressed numerically. Consequently, a computer program was developed and validated using a 3D finite element method simulation. The obtained results demonstrate a strong agreement between the two models under consideration, and they are also consistent with the experimental results conducted to validate the models. The advantage of the analytical approach used in the presented analyses lies in the very short calculation times, which are beyond comparison. Due to that, it was possible to determine the full operating characteristics of the thermoelectric module. The calculations were performed for four cases of the occurrence and distribution of contact resistance:

- Zero contact resistance $r_h = r_c = 0 \mu\text{Km}^2/\text{W}$ —the comparative case;
- Total contact resistance located on the hot side $r_h = 220 \mu\text{Km}^2/\text{W}$, $r_c = 0 \mu\text{Km}^2/\text{W}$;
- Total contact resistance located on the cold side $r_h = 0 \mu\text{Km}^2/\text{W}$, $r_c = 220 \mu\text{Km}^2/\text{W}$;
- The same contact resistance on both sides $r_h = r_c = 220 \mu\text{Km}^2/\text{W}$.

All simulations were conducted for a commercial thermoelectric module with parameters determined by our own experiment [36].

The results of the analyses of the thermoelectric generator show that a higher value of maximum power occurs for higher resistance on the cold side of the TEG. In this situation, the heat flux reaching the heat sink is smaller than the flux supplied by the heat source. The difference is carried to the outside in the form of electric power. On the other hand, the short-circuit current is higher for bigger resistances on the hot side because in this situation, the TEG average temperature is lower and so is the Peltier coefficient. Owing to that, a stronger current can flow through the system.

The results of the simulations prove that the magnitude of contact resistance has a significant impact on the obtained values of the electromotive force, the short-circuit current, and consequently, the TEG power and efficiency. It should be emphasized that, from a practical point of view, the most important factor in the case of the TEG is the total magnitude of the contact resistance and not its distribution. The higher resistance

on either side of the module leads to a shift in the average operating temperature of the thermoelectric junction towards the opposite side. This means, for example, that the deterioration in contact on the hot side will cause a drop in the module mean temperature as well as the temperature of each junction. For these reasons, the developed model can be successfully applied in cases of uneven deterioration in the contact quality between the module and the exchangers due, for example, to the operating temperature or in-service time.

The results also show that the greatest significance of contact resistance is observed at low values of the TEG thermal resistance, which is the effect of very short legs forming the thermoelectric couples. In commercial TEGs, the legs typically have a height of about 1–3 mm. The analyses conducted during this work prove that for such heights of the leg, the assumption of the contact resistance symmetry seems fully justified.

Considering the differences in the values of contact resistance on the two sides of the TEG, the numerator of the equation describing the maximum power is a current-dependent polynomial of the third degree. Nevertheless, the term at I^3 is usually so small that the curve illustrating the current-dependent changes in power can well be treated as parabolic with the apex of (P_{max}) occurring for half the short-circuit current ($I = 0.5I_{sc}$). The error is smaller than 1%, and the measurement of I_{sc} is very easy to carry out.

The conducted research demonstrates that the impact of thermal resistance in the thermoelectric system is significant for the majority of the analysed operational scenarios. This justifies taking actions to minimize this resistance, including the use of thermal grease, proper clamping force, module construction designed to limit this resistance, appropriate radiators, heat exchangers in the system, etc. It is also crucial to consider the potential degradation in thermal contact over time due to factors such as a decrease in clamping force, drying of thermal grease, or oxidation of the contact surface. The conclusion drawn from the analysis is that, in the case of TEGs, total resistances are important, with their location being less significant. For TECs, the value of the resistance on the heat release side is always important due to the high heat flow, while on the cold side, it matters only when significant cooling power needs to be provided. Neglecting thermal resistances can lead to significant errors in estimating TEG/TEC parameters or designing a thermoelectric system.

Author Contributions: Conceptualization, R.B.; methodology, R.B., I.N. and G.N.; software, R.B.; validation, R.B.; formal analysis, G.N.; investigation, R.B.; resources, G.N.; data curation, R.B., G.N. and I.N.; writing—original draft preparation, R.B. and I.N.; writing—review and editing, G.N.; visualization, G.N. and R.B.; supervision, G.N. and I.N.; project administration, G.N.; funding acquisition, R.B. and G.N. All authors have read and agreed to the published version of the manuscript.

Funding: This research was funded by statutory research funds for young scientists, Silesian University of Technology.

Data Availability Statement: Raw data will be available upon request. The data are not publicly available due to complexity of the datasheet structure.

Conflicts of Interest: The authors declare no conflicts of interest.

References

1. Pourkiaei, S.M.; Ahmadi, M.H.; Sadeghzadeh, M.; Moosavi, S.; Pourfayaz, F.; Chen, L.; Arab Pour Yazdi, M.; Kumar, R. Thermoelectric cooler and thermoelectric generator devices: A review of present and potential applications, modeling and materials. *Energy* **2019**, *186*, 115849. [[CrossRef](#)]
2. Zhang, A.B.; Wang, B.L.; Pang, D.D.; Chen, J.B.; Wang, J.; Du, J.K. Influence of leg geometry configuration and contact resistance on the performance of annular thermoelectric generators. *Energy Convers. Manag.* **2018**, *166*, 337–342. [[CrossRef](#)]
3. Marchenko, O.V. Performance modeling of thermoelectric devices by perturbation method. *Int. J. Therm. Sci.* **2018**, *129*, 334–342. [[CrossRef](#)]
4. Kim, S. Analysis and modelling of effective temperature differences and electrical parameters of thermoelectric generators. *Appl. Energy* **2013**, *102*, 1458–1463. [[CrossRef](#)]
5. Lv, S.; Liu, M.; He, W.; Li, X.; Gong, W.; Shen, S. Study of thermal insulation materials influence on the performance of thermoelectric generators by creating a significant effective temperature difference. *Energy Convers. Manag.* **2020**, *207*, 112516. [[CrossRef](#)]

6. Youn, N.; Lee, H.; Wee, D.; Gomez, M.; Reid, R.; Ohara, B. Achieving Maximum Power in Thermoelectric Generation with Simple Power Electronics. *J. Electron. Mater.* **2014**, *43*, 1597–1602. [[CrossRef](#)]
7. Karthick, K.; Suresh, S.; Singh, H.; Joy, G.C.; Dhanuskodi, R. Theoretical and experimental evaluation of thermal interface materials and other influencing parameters for thermoelectric generator system. *Renew. Energy* **2019**, *134*, 25–43. [[CrossRef](#)]
8. Ming, T.; Wu, Y.; Peng, C.; Tao, Y. Thermal analysis on a segmented thermoelectric generator. *Energy* **2015**, *80*, 388–399. [[CrossRef](#)]
9. Karana, D.R.; Sahoo, R.R. Influence of geometric parameter on the performance of a new asymmetrical and segmented thermoelectric generator. *Energy* **2019**, *179*, 90–99. [[CrossRef](#)]
10. Eldesoukey, A.; Hassan, H. 3D model of thermoelectric generator (TEG) case study: Effect of flow regime on the TEG performance. *Energy Convers. Manag.* **2019**, *180*, 231–239. [[CrossRef](#)]
11. Liao, T.; Xiao, J.; Xu, Y.; Lin, B. Thermal-electrical coupling properties and optimum analysis of a vehicle exhaust driven thermoelectric system. *Therm. Sci. Eng. Prog.* **2021**, *25*, 101040. [[CrossRef](#)]
12. Abderezzak, B.; Randi, S. Experimental investigation of waste heat recovery potential from car radiator with thermoelectric generator. *Therm. Sci. Eng. Prog.* **2020**, *20*, 100686. [[CrossRef](#)]
13. Wang, Y.; Li, S.; Xie, X.; Deng, Y.; Liu, X.; Su, C. Performance evaluation of an automotive thermoelectric generator with inserted fins or dimpled-surface hot heat exchanger. *Appl. Energy* **2018**, *218*, 391–401. [[CrossRef](#)]
14. He, W.; Guo, R.; Takasu, H.; Kato, Y.; Wang, S. Performance optimization of common plate-type thermoelectric generator in vehicle exhaust power generation systems. *Energy* **2019**, *175*, 1153–1163. [[CrossRef](#)]
15. Zaher, M.H.; Abdelsalam, M.Y.; Cotton, J.S. Study of the effects of axial conduction on the performance of thermoelectric generators integrated in a heat exchanger for waste heat recovery applications. *Appl. Energy* **2020**, *261*, 114434. [[CrossRef](#)]
16. Memon, S.; Tahir, K.N. Experimental and Analytical Simulation Analyses on the Electrical Performance of Thermoelectric Generator Modules for Direct and Concentrated Quartz-Halogen Heat Harvesting. *Energies* **2018**, *11*, 3315. [[CrossRef](#)]
17. Mahmoudinezhad, S.; Rezaia, A.; Rosendahl, L.A. Behavior of hybrid concentrated photovoltaic-thermoelectric generator under variable solar radiation. *Energy Convers. Manag.* **2018**, *164*, 443–452. [[CrossRef](#)]
18. Ge, Y.; Lin, Y.; He, Q.; Wang, W.; Chen, J.; Huang, S.M. Geometric optimization of segmented thermoelectric generators for waste heat recovery systems using genetic algorithm. *Energy* **2021**, *233*, 121220. [[CrossRef](#)]
19. Darkwa, J.; Calautit, J.; Du, D.; Kokogianakis, G. A numerical and experimental analysis of an integrated TEG-PCM power enhancement system for photovoltaic cells. *Appl. Energy* **2019**, *248*, 688–701. [[CrossRef](#)]
20. Tian, Y.; Liu, A.; Wang, J.; Zhou, Y.; Bao, C.; Xie, H.; Wu, Z.; Wang, Y. Optimized output electricity of thermoelectric generators by matching phase change material and thermoelectric material for intermittent heat sources. *Energy* **2021**, *233*, 121113. [[CrossRef](#)]
21. Bjørk, R.; Nielsen, K.K. The maximum theoretical performance of unconcentrated solar photovoltaic and thermoelectric generator systems. *Energy Convers. Manag.* **2018**, *156*, 264–268. [[CrossRef](#)]
22. Kossyvakis, D.N.; Voutsinas, G.D.; Hristoforou, E.V. Experimental analysis and performance evaluation of a tandem photovoltaic-thermoelectric hybrid system. *Energy Convers. Manag.* **2016**, *117*, 490–500. [[CrossRef](#)]
23. Kwan, T.H.; Wu, X.; Yao, Q. Complete implementation of the combined TEG-TEC temperature control and energy harvesting system. *Control Eng. Pract.* **2020**, *95*, 104224. [[CrossRef](#)]
24. Yuan, J.; Zhu, R. A fully self-powered wearable monitoring system with systematically optimized flexible thermoelectric generator. *Appl. Energy* **2020**, *271*, 115250. [[CrossRef](#)]
25. Lee, D.; Park, H.; Park, G.; Kim, J.; Kim, H.; Cho, H.; Han, S.; Kim, W. Liquid-metal-electrode-based compact, flexible, and high-power thermoelectric device. *Energy* **2019**, *188*, 116019. [[CrossRef](#)]
26. Fan, S.; Gao, Y.; Rezaia, A. Thermoelectric performance and stress analysis on wearable thermoelectric generator under bending load. *Renew. Energy* **2021**, *173*, 581–595. [[CrossRef](#)]
27. Shen, L.; Pu, X.; Sun, Y.; Chen, J. A study on thermoelectric technology application in net zero energy buildings. *Energy* **2016**, *113*, 9–24. [[CrossRef](#)]
28. Siddique, A.R.M.; Muresan, H.; Majid, S.H.; Mahmud, S. An adjustable closed-loop liquid-based thermoelectric electronic cooling system for variable load thermal management. *Therm. Sci. Eng. Prog.* **2019**, *10*, 245–252. [[CrossRef](#)]
29. Söylemez, R.; Alpman, E.; Onat, A.; Hartomacioğlu, S. CFD analysis for predicting cooling time of a domestic refrigerator with thermoelectric cooling system. *Int. J. Refrig.* **2021**, *123*, 138–149. [[CrossRef](#)]
30. Lyu, Y.; Siddique, A.R.M.; Majid, S.H.; Biglarbegian, M.; Gadsden, S.A.; Mahmud, S. Electric vehicle battery thermal management system with thermoelectric cooling. *Energy Rep.* **2019**, *5*, 822–827. [[CrossRef](#)]
31. Yu, J.; Hongji, Z.; Li, K.; Haoqing, W.; Jiawen, S.; Qingshan, Z. Analysis of Nonlinear Transient Energy Effect on Thermoelectric Energy Storage Structure. *Materials* **2020**, *13*, 3639. [[CrossRef](#)] [[PubMed](#)]
32. Nesarajah, M.; Felgner, F.; Frey, G. Modelling and simulation of a thermoelectric Energy Harvesting System for control design purposes. In Proceedings of the 16th International Conference on Mechatronics, Brno, Czech Republic, 3–5 December 2014; pp. 170–177. [[CrossRef](#)]
33. Tian, Z.; Lee, S.; Chen, G. Heat Transfer in Thermoelectric Materials and Devices. *ASME J. Heat Transf.* **2013**, *135*, 061605. [[CrossRef](#)]
34. Eivari, H.A.; Sohbatzadeh, Z.; Mele, P.; Assadi, M.H.N. Low thermal conductivity: Fundamentals and theoretical aspects in thermoelectric applications. *Mater. Today Energy* **2021**, *21*, 100744. [[CrossRef](#)]

35. Buchalik, R.; Nowak, G.; Nowak, I. Comparative analysis and optimization of one- and two-stage cooling systems with thermoelectric cells with respect to supercooling. *Energy Convers. Manag.* **2022**, *259*, 115587. [[CrossRef](#)]
36. Buchalik, R.; Nowak, G.; Nowak, I. Mathematical model of a thermoelectric system based on steady- and rapid-state measurements. *Appl. Energy* **2021**, *293*, 116943. [[CrossRef](#)]
37. Buchalik, R.; Nowak, G.; Nowak, I. Modelling transient states of thermoelectric systems. *Appl. Therm. Eng.* **2023**, *219*, 119647. [[CrossRef](#)]

Disclaimer/Publisher's Note: The statements, opinions and data contained in all publications are solely those of the individual author(s) and contributor(s) and not of MDPI and/or the editor(s). MDPI and/or the editor(s) disclaim responsibility for any injury to people or property resulting from any ideas, methods, instructions or products referred to in the content.